Analyzing density-driven errors: Principles and pitfalls

Sehun Kim[a], Do-gyeong Lee[a], Gyumin Kim[a], Youngsam Kim[a],
Mihira Sogal[b], Steven Crisostomo[c], Kieron Burke[b,c], and Eunji Sim[a*]
[a]Department of Chemistry, Yonsei University, 50 Yonsei-ro Seodaemun-gu, Seoul 03722, Korea.
[b]Department of Chemistry, University of California, Irvine, CA 92697, USA
[c]Department of Physics and Astronomy, University of California, Irvine, CA 92697, USA

February 22, 2026

Abstract

The theory of density-corrected density functional theory (DC-DFT) separates the error in any approximate DFT calculation into a functional-driven contribution and a density-driven error. Practical DC-DFT calculations often use the Hartree-Fock density instead of a self-consistent DFT density–a method known as HF-DFT–and reduce energetic errors in several classes of chemical problems. Using principles of DC-DFT, we illustrate several pitfalls when analyzing HF-DFT errors, including an interpolator for density-driven errors that is chronically inaccurate, using proxies instead of accurate densities, and conflating common measures of density errors with those of DC-DFT. We report ideal density-driven errors for one- and two-electron systems, where we can calculate most properties exactly, illustrating these problems. A simple analysis of benchmarking data shows that proxy benchmark densities proposed in recent literature are too inaccurate to be useful in DC-DFT. We argue that the success of HF-DFT for barrier heights need not rely on error cancellation. While HF-DFT errors can indeed be smaller than functional errors, the reason for the remarkable consistency of this improvement remains an open question.

I. Introduction

Kohn-Sham Density Functional Theory (KS-DFT)[1] is a widely used approach in computational chemistry due to its balance of accuracy and computational efficiency. Density-corrected DFT (DC-DFT)[2] is a general theoretical framework for separating errors in any DFT calculation into two well-defined contributions: a functional error and a density-driven error. A wide range of studies on DC-DFT have been actively conducted by different research groups, covering diverse approaches and systems.[3–27] The total errors of most DFT calculations are dominated by functional errors, but several specific classes of DFT calculations have been found to have significant density-driven errors. In such cases, the simple expedient of using the Hartree-Fock (HF)[28] density in place of the self-consistent DFT density–referred to as HF-DFT–often reduces the error, sometimes quite substantially. This effect is sometimes lost in the overall statistics because only a small subset of reactions are density sensitive.[8] Nonetheless, the overall performance of the weighted total mean absolute deviation (WTMAD-2) measure of error on the GMTKN55[29] database (general-main group thermochemistry, kinetics, and noncovalent interactions) of many standard functionals is significantly improved by use of HF densities[21,22,30,31], when the principles of DC-DFT are applied, including when dispersion corrections are modified to account for DC-DFT.[15,21]

The obvious explanation for the success of DC-DFT using HF densities in density-sensitive problems is that (a) the HF density is physically more sound and much closer to the exact density than the self-consistent DFT density, and (b) the removal of density-driven errors substantially reduces the overall error. This has been demonstrated in the original application of electronegativity calculations, with the prototype case being that of hydrogen[2], as well as for stretched heteronuclear bonds[4–6]. For such extreme cases, it has long been known that density functional approximation methods often exhibit convex behavior rather than adhering to the piecewise-linear behavior (PPLB condition)[32] for fractional charges, leading to spurious charge transfer. Density-driven errors overlap with, but are not identical to, delocalization errors. After all, stretched H_2^+ is the prototype self-interaction error,[33] but those are functional-driven contributions for standard semilocal approximations, not density-driven. The prototypical density-driven error is anions, where a truly self-consistent KS calculation with a semilocal approximation typically loses about 0.3 electrons.[4]

Several recent papers[20,23,25,26] have questioned this explanation in other cases, especially in the high-profile case of transition-state barriers, water clusters, and halogen and chalcogen complexes. These papers argue that the improved energy of HF-DFT is due to the use of an overlocalized HF density, which changes the sign of the density-driven error of

*esim@yonsei.ac.kr

the delocalized approximate functional, causing cancellation with the functional error. They claim that density-driven errors of HF densities are much greater than those of self-consistent densities, which implies a substantial and unconventional cancellation of functional and density-driven errors when the HF density is used. Some of these claims are based on proxies for benchmark densities, and others depend on an interpolation formula of questionable applicability. But by performing KS inversions, it has definitively been shown for one particular barrier (both forward and backward) that the density-driven error is only a small fraction of the total error in the barrier height. A similar result has recently appeared for another barrier[34].

The purpose of the present work is to examine these claims rigorously in terms of the basic principles of DC-DFT. We include three different kinds of investigation: theoretical, calculations on simple models, and practical calculations of molecular systems. In the theoretical category, we point to several key principles and derive several new formulas. However, the most relevant definitions and formulas require knowledge of the exact XC functional for arbitrary densities. Hence, the second category involves model systems, where we do know the exact functional and can test these formulas and compare the results to pragmatic approximations. In the third category, we do as much as we practically can to relate pragmatic results to the more ideal cases. Unfortunately, without the machinery to calculate some of these results for realistic cases, we are unable to resolve the key question of how HF-DFT is lowering DFT energy barrier errors in terms of DC-DFT. However, we provide several additional results that help contextualize this issue and clarify how it has been discussed in the literature.

First, we answer a question raised by Savin[35], who pointed out that the density-driven error of DC-DFT (called pragmatic here) depends on the approximate functional. Briefly defined, the (pragmatic) density-driven error is the energy difference between an approximate XC functional evaluated at its self-consistent density minus its value on the exact density. The corresponding ideal density-driven error, being the difference between the exact functional evaluated on the two densities, does not depend on any energy approximation (Sec. III1). We show in many one-electron cases and in the Hubbard dimer that in fact the pragmatic density-driven error is an excellent approximation to the ideal, strongly suggesting that this is not an issue in practical DC-DFT. In fact, it was already argued in Eqs. 47-48 of Ref.[36] that the pragmatic density-driven error closely estimates the ideal, provided that the approximate functional in question has the correct curvature about its minimum.

Perhaps contrary to expectation, the density of an HF-DFT calculation is NOT the HF density itself. Specifically, the true density of an HF-DFT calculation—defined as the self-consistent density of an approximate functional that yields the HF-DFT energy for every potential—is distinct from the HF density. We explicitly write down the difference terms, but unfortunately cannot evaluate them for realistic systems. One can also define the corresponding HF-DFT functional, $E_{\rm XC}^{\rm HF-DFA}[n]$, which, if inserted in the KS equations, would yield both the energy and true density of an HF-DFT calculation. In model systems, we can only perform the calculation for a mimic of HF-DFT. But in such cases, we show that, when we evaluate a DFA on an approximate (not self-consistent) density yielding an improved energy, the true density of that calculation can in fact be more accurate (in the DC-DFT sense) than either the self-consistent or the approximate density. Since this can happen in the model calculation, it is a possible explanation for the results of HF-DFT in realistic cases, but we have no way to check at present for practical calculations. In any event, this shows that the accuracy of the HF density itself might not be the correct quantity to focus on.

Our model calculation also shows that an interpolation scheme used in Refs.[20,23,25,26] to measure density-driven errors of densities other than a self-consistent density, can be quite inaccurate. Such estimates of the density-driven error of HF-DFT calculations are unlikely to be quantitatively meaningful.

The original work[20] showing issues for barrier heights did not include a KS inversion, but instead relied on three approximate DFT schemes to generate proxies for benchmark densities, and subsequent work has cited this as evidence for small density-driven errors in these systems. However, we show that, even measured by internal consistency, these proxy benchmark densities are insufficiently accurate to yield useful estimates of density-driven error. In fact, in a theoretical development, their errors can be directly related to the failures of the interpolation scheme mentioned above.

Many authors have chosen various plausible measures of density differences and find many systems where HF densities are less accurate than self-consistent densities by such measures, which suggests some issue with using HF-DFT to reduce DFT errors. We spend considerable effort in trying to find any such measure that can be generally related to the density-driven errors of DC-DFT, but can find none. Apparent inaccuracies of HF densities relative to self-consistent densities are irrelevant to DC-DFT for several reasons. First, DC-DFT is primarily concerned with energy differences, such as barrier heights, which are not simply related to density differences. Second, as mentioned above, the self-consistent density of an HF-DFT calculation is known not to be the HF density, and so the quality of the HF density is not the correct measure. (In the cases dominated by delocalization error in the density, we know the HF density itself is better, in the sense of DC-DFT.)

Based on this analysis, we propose an alternative interpretation for the success of HF-DFT. The true density-driven error

in HF-DFT is likely much smaller than previously estimated via the interpolator. The observed improvement in accuracy, therefore, may stem not from a cancellation of large errors, but primarily from a reduction in the functional-driven contribution. As our 1-electron models illustrate, using a more accurate density (like HF) shifts the evaluation to a region of density space where the approximate functional itself performs more accurately. This phenomenon is consistent with DC-DFT principles and would explain why HF-DFT errors can be smaller than the functional error. But we cannot currently validate this explanation for practical HF-DFT calculations.

The remainder of this paper is organized as follows. Section II establishes the theoretical background and defines the main sources of error in density functional calculations. Section III develops a formal framework to distinguish different types of density-related errors and clarifies their conceptual roles. Section IV tests these ideas in simple model systems to illustrate their behavior. Section V extends the discussion to molecular examples and examines how practical challenges arise when accurate benchmark densities are unavailable. Section VI analyzes reaction barrier heights using pragmatic definitions, highlighting that density-sensitive reactions exhibit imbalanced errors between reactants and products, and that commonly used density metrics show no clear correlation with the pragmatic error measure. Finally, Section VII summarizes the key findings and discusses their implications for the broader understanding and application of density-corrected approaches.

II. Background

II1. Principles

Most ground-state electronic structure methods are primarily used to extract E_v, the ground-state energy as a functional of the one-body potential $v(\mathbf{r})$. Chemical reaction energies are the differences in energies for two different potentials. Derivatives with respect to nuclear positions determine forces, vibrations, and equilibrium geometries. Given its importance, almost all such methods have been tuned to optimize accuracy in energies. The Rayleigh-Ritz variational principle states[37]:

$$E_v = \min_{\Psi} \langle \Psi | \hat{H}_v | \Psi \rangle \tag{1}$$

where the minimization is over all antisymmetric wavefunctions with N electrons, and $\hat{H}_v$ is the electronic Hamiltonian. In fact, even the density can (in principle) be extracted directly from a sequence of such calculations via

$$n_v(\mathbf{r}) = \frac{\delta E_v}{\delta v(\mathbf{r})} \tag{2}$$

for a given N (subject to certain concavity conditions to ensure it exists[38]). A KS-DFT calculation writes the variational principle in terms of the density:

$$E_v = \min_{n} E_v[n] = E_v[n_v], \tag{3}$$

where the minimization is over all (Lieb-allowed[39]) densities integrating to N and

$$E_v[n] = T_{\rm S}[n] + U[n] + E_{\rm XC}[n] + \int d^3r \; n(\mathbf{r})\, v(\mathbf{r}). \tag{4}$$

Here $T_{\rm S}$ is the KS kinetic energy, U the Hartree energy, and $E_{\rm XC}$ is the exchange-correlation (XC) energy, which is approximated in practical calculations. The self-consistent solution of the KS equations performs precisely the minimization of Eq. 3. Moreover, at self-consistency, the KS density is exactly equal to that of Eq. 2, by construction. In reality, all modern DFT calculations are spin-density calculations[40], but we give formulas in terms of the total density for simplicity. We also use energy units of Hartrees for one- and two-electrons systems and for real systems later use kcal/mol. Distances are in Å unless otherwise noted.

With exact density $n_v(\mathbf{r})$ and exact ground-state energy $E_v[n_v]$, the (total) energy error (TE) of any self-consistent DFT calculation is:

$$\Delta\widetilde{E}_v = \widetilde{E}_v[\tilde{n}_v] - E_v[n_v], \tag{5}$$

where $\tilde{n}_v(\mathbf{r})$ is the self-consistent density of a given approximate functional $\widetilde{E}_v$. In DC-DFT this error is split into two well-defined contributions,

$$\Delta\widetilde{E}_v = \Delta\widetilde{E}_{\rm F} + \Delta\widetilde{E}_{\rm D}. \tag{6}$$

The functional error (FE) is

$$\Delta\widetilde{E}_{\rm F} = \widetilde{E}_v[n_v] - E_v[n_v], \tag{7}$$

i.e., the error the approximate functional $\widetilde{E}_v$ makes on the exact density $n_v(\mathbf{r})$. If the approximate calculation is a KS calculation with an approximate XC functional, $\widetilde{E}_{\rm XC}[n]$, its error is a pure density functional of any density $n(\mathbf{r})$

$$\Delta E_{\rm XC}[n] = \widetilde{E}_{\rm XC}[n] - E_{\rm XC}[n], \tag{8}$$

and the functional error is just that functional on the exact density:

$$\Delta\widetilde{E}_{\rm F} = \Delta E_{\rm XC}[n_v]. \tag{9}$$

The remaining error is defined as the pragmatic density-driven error (pragmatic-DDE):

$$\Delta\widetilde{E}_{\rm D} = \widetilde{E}_v[\tilde{n}_v] - \widetilde{E}_v[n_v]. \tag{10}$$

We adopt the qualifier 'pragmatic' for this quantity (which in our previous work was referred to simply as the density-driven error) to explicitly distinguish it from the corresponding ideal-DDE that will be introduced in Sec. III1. Most DFT errors

are dominated by the functional error, which we call *normal*. In some systems, the pragmatic-DDE can nonetheless play a significant role. Such calculations were originally labeled *abnormal*, and could be spotted by a small HOMO-LUMO gap.[2] These were later found to be sufficient but not necessary conditions. In particular, more accurate functionals would often have smaller errors, not dominated by gaps, but still significantly reduced by using better densities. In this work specifically, we refer to Eqs. 7 and 10 as pragmatic errors. By the variational principle, pragmatic-DDEs of total energy are always negative. We use the term "benchmark density" exclusively to denote a high-level, benchmark-quality density (e.g., CCSD[41,42]), in contrast to the exact density, which is not available in practice. Throughout, we assume any difference between such densities and exact densities is negligible.

Several points are worth noting. First, while all these formulas have been given for the total energy of a specific moiety, in practice, they are applied to the energy differences that are used in chemical and material calculations. A second point is that the HF density has not been mentioned. These are general formulas that in principle can be applied to any system, if the ingredients are available (usually highly accurate energies and densities). We also note that pragmatic-DDEs are only defined using the self-consistent density $\tilde{n}_v(\mathbf{r})$ of a given approximate $\widetilde{E}_{\mathrm{XC}}$, because the variational principle is hard-wired into their definition[2,36]. Finally, we mention that this pragmatic-DDE depends both on the system and the approximate functional in use.

For any potential $v(\mathbf{r})$ and approximate functional, we define the following density functional

$$\widetilde{D}_v[n] = \widetilde{E}_v[n] - \widetilde{E}_v[n_v]. \tag{11}$$

Here we call this quantity the energetic density interpolator (EDI). While generally applicable to any arbitrary density $n(\mathbf{r})$, it specifically matches the pragmatic-DDE if $n(\mathbf{r})$ is the self-consistent density of $\tilde{E}_v$ and vanishes if $n(\mathbf{r})$ is the exact density $n_v(\mathbf{r})$. This formula was defined in Ref.[36] in Eqs. 18 and 19 under the name "density-driven difference", but here we will show it bears little relation to density-driven errors if applied to non-self-consistent densities, such as the HF density. Most importantly, it does not yield the pragmatic-DDE of a HF-DFT calculation.[7,20,23,25,26,43] Our functional applies to any approximate density, but in the specific case where $n(\mathbf{r})$ is the HF density, this quantity is identical to the non-variational density over-localization defined in Ref.[26].

II2. Practicalities

If DC-DFT always required using the exact density, it would not be very useful. In most practical DC-DFT calculations, the (unrestricted) HF density is employed as a pragmatic choice for implementing density correction, since it is generally assumed to be more reliable than the self-consistent density in abnormal situations.[44] In fact, one usually finds that HF densities do little harm in *normal* calculations, so one can often use them everywhere.[31] Such calculations are dubbed HF-DFT. They pre-date DC-DFT, but largely because originally DFT was tested on HF densities[45–48], assuming DDEs were irrelevant. While they significantly improve energetics for abnormal calculations, they have the practical drawback of being non-variational, and therefore require additional response terms (beyond the Hellmann–Feynman term) to compute forces.[13,48] Moreover, if the UHF calculation is highly spin contaminated, that suggests its density is not accurate, and restricted open-shell HF (ROHF) densities are used instead.[31]

Almost all DC-DFT calculations reported have been for molecular systems. Specific examples include reaction barrier height[47,48], torsional barrier[10], halogen and chalcogen bonds[6,19], anions[3], most stretched bonds[4,5], water simulation[9,11,12,14–16,24,49], and many other chemical properties[13,17,18,27]. A practical criterion to assess abnormality in DC-DFT is to compute the density sensitivity ($\widetilde{S}$),[50] which is defined as the difference in energy obtained by evaluating the approximate functional on two qualitatively different densities[32]—typically those from HF and the local density approximation (LDA):

$$\widetilde{S} = \left| \widetilde{E}[n^{\mathrm{LDA}}] - \widetilde{E}[n^{\mathrm{HF}}] \right| \tag{12}$$

A large $\tilde{S}$ value indicates that the approximate functional's energy is highly sensitive to the change of density. In such a case, if the functional produces a problematic self-consistent density, that density is likely to be significantly reflected in the energy. Conversely, if $\tilde{S}$ is small (insensitive), the density is unlikely to contribute significantly to the total energy error. A DFT calculation is considered density sensitive if $\widetilde{S} > 2$ kcal/mol, suggesting that density-correction may change the energetics. Conversely, if $\widetilde{S} < 2$ kcal/mol, the system is deemed density insensitive, and the choice of density has minimal impact on the energy. Which reactions are density-sensitive depends on the choice of approximate functional. We emphasize that the value of 2 kcal/mol is a practical guideline rather than a universal threshold.[17,44,51] It is important to note the size-extensivity of $\tilde{S}$; for larger systems, the density sensitivity naturally increases. While the current metric works reasonably well for small molecules, normalized criteria are required to extend it to larger systems, and several studies have suggested potential approaches for such normalization.[52,53] Of course, it is irrelevant if one has access to the exact functional and density, as then the ideal-DDE (defined later in Sec. III1.) itself can be calculated directly.

An important aspect of DC-DFT is that the accuracy of the density is measured solely in terms of energy. Because density is a function, one can construct infinitely many different measures of the accuracy of a density.[54] But if errors in densities do

not translate into significant errors in energy, they are of little practical importance in DFT calculations.[50] By measuring accuracy in terms of energies, one can automatically see the relevance to DFT applications. Despite its name, applications of DFT mostly involve reports of energies as a function of nuclear coordinates. Thus, an important concept introduced by DC-DFT is the idea of measuring density errors in terms of the actual energy errors reported in calculations. This is the conceptual cornerstone of the theory, and has also been the key to its practical success.

A crucial part of this paper will be the question: What is the pragmatic-DDE of a HF-DFT calculation? A plausible estimate is simply to apply the EDI to the HF density. Some of us even carelessly used that in Fig. 4 of Ref.[7], without carefully distinguishing it from a proper DDE. But this is NOT the correct formula for the pragmatic-DDE of HF-DFT. In Ref.[36] (Eqs. 47-48) it was shown that the pragmatic-DDE (Eq. 10) should give a good estimate of the ideal-DDE *only for self-consistent calculations*. However, we can still conceptualize the pragmatic-DDE of a HF-DFT calculation by imagining an approximate XC functional which, at self-consistency, yields the exact same energy as HF-DFT. We call the minimizing density of this functional the "self-consistent density of the inconsistent calculation". In principle, it could be calculated by writing the HF-DFT energy as:

$$\widetilde{E}_v^{\mathrm{HF-DFT}} = E_v^{\mathrm{HF}} + \widetilde{E}_{\mathrm{XC}}[n^{\mathrm{HF}}] - E_{\mathrm{X}}^{\mathrm{HF}}[n^{\mathrm{HF}}]. \qquad (13)$$

and inserting this into Eq. 2 to find:

$$n^{\mathrm{HF-DFT}}(\mathbf{r}) = n^{\mathrm{HF}}(\mathbf{r}) + \frac{\delta(\widetilde{E}_{\mathrm{XC}}[n_v^{\mathrm{HF}}] - E_{\mathrm{X}}^{\mathrm{HF}}[n_v^{\mathrm{HF}}])}{\delta v(\mathbf{r})}. \qquad (14)$$

This density is *not* the same as the HF density. It includes a complicated correction to the HF density that is impractical to calculate, and is omitted if using the EDI of Eq. 11. In our one-electron examples in Sec. IV, we calculate the self-consistent densities of inconsistent calculations, and show that they are considerably different from the surrogate density on which the functional is evaluated.

The results of the present work suggest that applying the EDI directly to the HF density, rather than using Eq. 14, can yield highly unreliable estimates and may compromise the resulting conclusions.

III. Theory

III1. Ideal density-driven errors

Here we introduce the concept of the ideal density-driven error (ideal-DDE). Related constructions were explored independently in both Savin's group[35] and in our own prior work.[36,50]

In this manuscript we adopt the explicit label 'ideal-DDE' to make its role within DC-DFT unambiguous: it is the formal error associated with the density itself. For any potential $v(\mathbf{r})$, it is a density functional defined as:

$$\Delta E_{\mathrm{D}}^*[n] = E_v[n] - E_v[n_v]. \qquad (15)$$

Like the pragmatic definition, because it is energy-based, it fits just as well with the aims of DC-DFT. But it has two key advantages relative to the pragmatic definition: (a) it is a measure for any density considered as a trial density for a given system, no matter what its origin, and (b) it does not use an approximate functional for its evaluation. The pragmatic definition applies *only* to self-consistent densities of KS calculations, and uses the approximate functional in its evaluation. The energetic measure of the size of the pragmatic-DDE depends crucially on the accuracy of the approximate functional for that density. The ideal-DDE does not have this flaw, and is a simple metric for measuring the energetic distance of any approximate density for a given potential.

This concept was introduced in Ref.[50], but just as an abstraction, and a few of its formal properties were then listed in Ref.[36]. However, it has not previously been calculated. In practice, however, the ideal-DDE cannot be evaluated for realistic systems because it requires knowledge of the exact XC functional and the exact density, which are unavailable; its usefulness therefore lies primarily in conceptual analysis and model validation. Two exact properties are useful here. First, the ideal-DDE of the total energy is never negative, by the variational principle. This is the mirror image of the negativity of the pragmatic-DDE. The difference in sign is due to the exact functional being used. (We will see below that, for good approximations, $\Delta E_{\mathrm{D}}^*[\tilde{n}_v] \approx -\Delta \widetilde{E}_{\mathrm{D}}[\tilde{n}_v]$). Second, the ideal-DDE is also convex, i.e., if $n_\lambda(\mathbf{r}) = (1-\lambda)n_0(\mathbf{r}) + \lambda n_1(\mathbf{r})$, then

$$\Delta E_{\mathrm{D}}^*[n_\lambda] \leq (1-\lambda)\Delta E_{\mathrm{D}}^*[n_0] + \lambda \Delta E_{\mathrm{D}}^*[n_1], \quad 0 \leq \lambda \leq 1. \qquad (16)$$

Moreover, if $n_1(\mathbf{r})$ is the exact density, the second term vanishes.

However, it is very difficult to calculate this ideal-DDE for most electronic systems because we don't know the exact functional E_{XC}. Given an approximate density, one must guess the one-body potential (which typically is not Coulombic) for which this is a ground-state density, and find its ground-state energy. The only real-space case in which such calculations were done is Ref.[55], which is a one-dimensional simulacrum of a four H-atom chain. So, in general, such interacting inversions are impractical.

Here, we report such calculations in two special cases where they are feasible. The first is any one-electron system, where we can easily invert the Schrödinger equation for a trial density, and the second is the two-site Hubbard model with 2 fermions,

Table 1: Summary of symbols, acronyms, definitions, equations, and equation numbers throughout this paper.

symbol	acronym	definition	equation	eq.#
$\Delta E^*_{\rm D}[n]$	ideal-DDE	ideal density-driven error	$E_v[n] - E_v[n_v]$	Eq. 15
$\Delta \widetilde{E}_{\rm D}$	pragmatic-DDE	pragmatic density-driven error	$\widetilde{E}_v[\tilde{n}_v] - \widetilde{E}_v[n_v]$	Eq. 10
$\widetilde{D}_v[n]$	EDI	energetic density interpolator	$\widetilde{E}_v[n] - \widetilde{E}_v[n_v]$	Eq. 11
$\widetilde{\mathcal{E}}_{\rm D}[\tilde{n}; n_{proxy}]$	proxy-DDE	density-driven error with proxy benchmark density	$\widetilde{E}_v[\tilde{n}] - \widetilde{E}_v[n_{proxy}]$	Eq. 21
$\Delta E_{\rm XC}[n]$	XC energy deviation	exchange-correlation energy deviation	$\widetilde{E}_{\rm XC}[n] - E_{\rm XC}[n]$	Eq. 8
$\Delta \widetilde{E}_{\rm F}$	FE	functional error	$\widetilde{E}_{\rm XC}[n_v] - E_{\rm XC}[n_v]$	Eq. 7
$\Delta \widetilde{E}_v$	TE	total error	$\widetilde{E}_v[\tilde{n}_v] - E_v[n_v]$	Eq. 5

which is used to mimic two-electron systems and illustrate basic theory in DFT.[55]

How does this ideal-DDE compare to the pragmatic definition of Eq. 10? We show in the illustrations in this paper that often a good approximate functional has a pragmatic-DDE that is close to the negative of the ideal-DDE. (The sign flip is simply because the reference functional has changed from the approximate to the exact.) We give a condition that guarantees this, and most approximations in most calculations seem to meet this condition. When that condition is met, the difference between the functional error and the ideal-DDE yields approximately the total error. Table 1 provides a summary of the different types of errors discussed in this work, including symbols, acronyms, definitions, equations, and equation numbers.

III2. Measuring density errors

DDEs involve a finite difference of a given functional on two (presumably) very similar densities. These energy differences are typically smaller than the energy errors made by density functional approximations for chemical energy differences. Determining if methods are sufficiently accurate, and have been sufficiently well-converged with respect to a basis set, is highly non-trivial. Many of these issues are discussed in detail in Ref.[7].

As noted in a previous section, highly accurate methods such as coupled-cluster have been developed to yield accurate energy differences between configurations of atoms. We know of no systematic study that checks the accuracy of the corresponding density (and what would one check it against, anyhow?). Throughout the present work, we assume that the CCSD densities for small systems are sufficiently accurate as to introduce negligible error in calculating pragmatic-DDEs.

As a practical implementation of DC-DFT, HF densities are commonly used as proxies for the exact density. Here, we refer to such densities as *practical proxies*, meaning that their computational cost is not typically much higher than, e.g., a hybrid DFT calculation itself. The recent literature has suggested several other densities that are used in place of accurate densities, to test the efficacy of DC-DFT. We call these *proxy benchmark densities*. Clearly, to be useful in DC-DFT at all, these proxy benchmark densities should introduce errors in DDEs that are significantly smaller than the DDEs themselves. Ideally, they should have errors much smaller than the ideal-DDE of HF and self-consistent densities. We shall see that this is an extremely difficult standard to meet in practice (see section V1).

As has already been mentioned, DC-DFT provides just one of infinitely many ways of measuring errors in densities. But because chemical reaction energies are in fact energy differences of different configurations of nuclei, pragmatic-DDEs are typically only reported for such differences. In many such calculations, total energies of the individual moieties are unlikely to be well converged, as differences converge much faster with respect to the basis set. But most other measures of density error that appear in the literature apply only to the density of a given moiety, not the density difference when nuclei are rearranged. Measures that apply only to densities, and not differences of densities, are difficult (if not impossible) to relate directly to the efficacy of DC-DFT. From a different perspective, this is one of the huge benefits of the DC-DFT DDE construction - that it can be applied directly to the energy differences that are all important in applications.

III3. Functional interpolation

For any given approximate XC functional, we can imagine a one-dimensional family of XC approximations:

$$\widetilde{E}_{{\rm XC},a}[n] = (1-a)\,\widetilde{E}_{\rm XC}[n] + a\,E_{\rm XC}[n]. \tag{17}$$

For $0 \le a \le 1$, this interpolates between the approximate ($a = 0$, $\widetilde{E}_{\rm XC}$) and exact ($a = 1$, $E_{\rm XC}$) functionals. Solving the KS equations with this functional yields an approximate density $n_a(\mathbf{r})$ parameterized by a. If we extend the construction to any real value of a, this defines a one-dimensional line in density space, and the interpolation is the line segment where a runs from 0 to 1. For sufficiently accurate XC approximations, one would expect the density to vary approximately linearly with a between 0 and 1, but also to always be able to find extreme values of a where non-linearities are noticeable. For simple cases (one-electron), we can find the exact XC functional,

but not in practical applications of DC-DFT. Note also that different approximate XC functionals yield distinct families of densities, which coincide only at $a = 1$.

IV. Results for model systems

IV1. One electron systems

This section reports DC-DFT results for one-electron systems only. Inspired by recent studies[56,57] from the Goerigk group that analyze one-electron self-interaction and its manifestation in the density, we regard these systems as ideal test cases. This is because the exact functional is easy to calculate in this case, by simply doing a HF calculation, which is self-interaction free. This in turn allows us to perform self-consistent calculations for the functional interpolation (Eq. 17) of any approximate functional, and output its self-consistent density $n_a(\mathbf{r})$. Almost all the ideal- and pragmatic-DDEs reported here are negligible, so DC-DFT has little practical benefit. But the results demonstrate general principles that cannot be deduced from practical calculations.

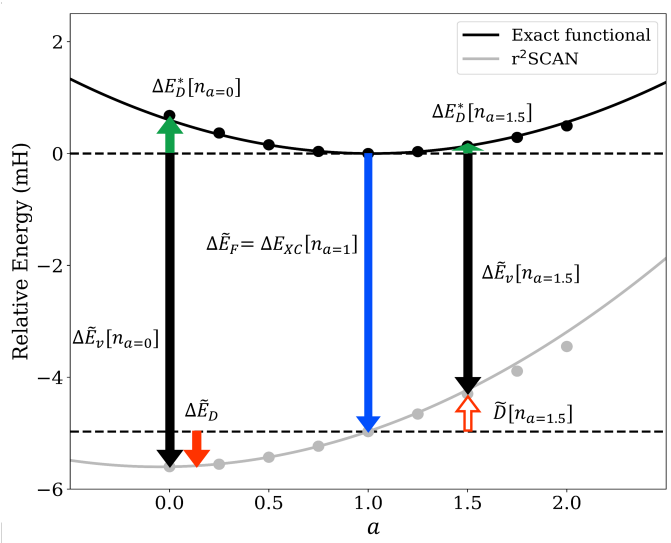

Figure 1: Energy curves of H_2^+ at equilibrium for r^{2}SCAN (gray) and exact functional (black) evaluated on the self-consistent densities of the functionals determined by the a in Eq. 17. The x-axis denotes the self-consistent densities with respect to the parameter a in Eq. 17. The solid arrows are the total (TE, black, Eq. 5), pragmatic density-driven (pragmatic-DDE, red, Eq. 10), and functional (FE, blue, Eq. 7) errors for r^{2}SCAN, with ideal-DDE in green. The red hollow arrow is $\widetilde{D}[n_{a=1.5}]$, a terrible approximation to (minus) its ideal-DDE (right green arrow, Eq. 15). Any density with $0 < a < 2$ is more accurate than r^{2}SCAN's, and all $1 < a < 2$ have *smaller* TEs (right, black) than the FE of the self-consistent r^{2}SCAN.

Figure 1 is the most important figure of this paper, and explains a significant fraction of its basic message. These are energy curves for H_2^+ at equilibrium (geometries of one-electron systems are provided in Table S1), using the r^{2}SCAN[58] functional, but are typical of many systems and many approximate functionals (more examples are shown in the Figs. S1-S5). The x-axis is a in Eq. 17 and the density at each value is the self-consistent density ($n_a(\mathbf{r})$) with that a. The solid black curve is the exact energy for each density, with the zero chosen at the exact energy, and the solid gray curve is the r^{2}SCAN energy. The black and red arrows on the left ($a = 0$) denote total error and pragmatic-DDE, respectively. While the blue arrow in the middle ($a = 1$) denotes the functional error of r^{2}SCAN.

The first point to note is that the value of the black curve is the ideal-DDE for each of the densities. To the extent that these densities are linear in a, this curve must be convex and typically is close to a simple parabola. Next we note that $\Delta E_{\rm D}^*[\tilde{n}] \approx -\Delta\widetilde{E}_{\rm D}$. We will show numerous systems and functionals where this is true to within about 20 %. Figure 2 shows the density errors with respect to exact density, as a function of a, which are clearly (almost) proportional to $1 - a$. Assuming linearity, this implies that the black-(exact)-curve in Fig. 1 is convex, as in Eq. 16. Moreover, it must always be parabolic on a small enough scale around $a = 1$. The closer the self-consistent density is to the exact density, the closer the ideal-DDE curve will be to a parabola.

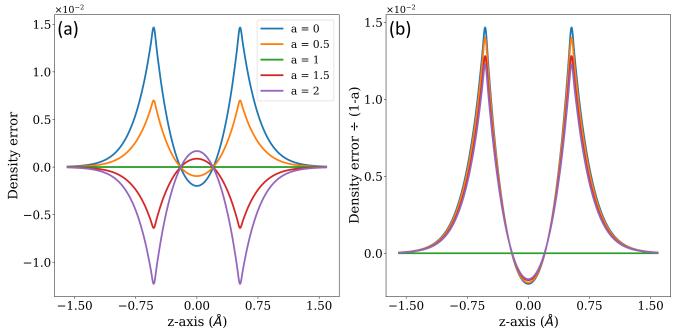

Figure 2: (a) Density errors of r^{2}SCAN from Eq. 17 and (b) density errors$\div(1-a)$ of H_2^+ at equilibrium along z-axis.

Another key point is that all densities with a between 0 and (about) 2 are more accurate than the self-consistent density ($a = 0$). i.e., they have smaller ideal-DDEs. In Table 2, we list three formulas for DDEs as a function of a (more examples are shown in Tables S2-S6). The first is the ideal. The second is the pragmatic, using the appropriate a-dependent functional for each value of a, as given by Eq. 10. It tracks the ideal very well, as expected. But the third uses the original functional ($a = 0$) to estimate the pragmatic-DDE at the intermediate points via Eq. 11, i.e., the EDI. While it is indeed correct at the two points ($a = 0$, and 1), it becomes more and more relatively inaccurate as a approaches 1, and nonsensical for $a > 1$, as its estimate of the pragmatic-DDE has the wrong sign!

Table 2: Ideal- and pragmatic-DDEs (prag.), and energetic density interpolator (EDI) in mH for H_2^+ at equilibrium, evaluated on the self-consistent densities of the functionals determined by the parameter a in Eq. 17. The pragmatic-DDE values are evaluated using the functional in Eq. 17 corresponding to each a, whereas the EDI values are evaluated only using the fixed r^{2}SCAN functional for each density.

(mH)	value of a								
type	0.00	0.25	0.50	0.75	1.00	1.25	1.50	1.75	2.00
ideal	0.68	0.37	0.16	0.04	0.00	0.03	0.13	0.29	0.49
prag.	-0.63	-0.35	-0.15	-0.04	0.00	-0.04	-0.14	-0.31	-0.53
EDI	-0.63	-0.58	-0.46	-0.26	0.00	0.31	0.68	1.08	1.52

Consider the functional with $a = 0.75$ and its associated density. Its ideal-DDE is much smaller than that of the self-consistent density, and the r^{2}SCAN functional evaluated on this density, $n_{a=0.75}(\mathbf{r})$, almost exactly reproduces the functional error, precisely as the naive understanding of DC-DFT expects. However, a more interesting comparison is with $a = 1.5$. This is still a much better density than the self-consistent density. But now the total error r^{2}SCAN makes on this density, $n_{a=1.5}(\mathbf{r})$, is even smaller than the functional error ($|\Delta\widetilde{E}_v[n_{a=1.5}]| < |\Delta E_{\rm XC}[n_{a=1}]|$). This is simply because $a > 1$ and the difference between the two curves, that is, $\Delta E_{\rm XC}[n_a]$ continues to shrink.

However, suppose we imagined that the EDI (Eq. 11) was an accurate measure of pragmatic-DDE. Its estimate of the pragmatic-DDE of $n_{a=1.5}(\mathbf{r})$ has the wrong sign, and is a large overestimate (red hollow arrow upwards in Fig. 1), compared with the tiny green arrow at $a = 1.5$. For this density, it appears that the pragmatic-DDE is *larger* than that of the self-consistent density, and that its removal leads to a smaller energy error, a highly fortuitous cancellation of errors with functional error that only gets better as a increases. However, as we can see, the ideal-DDE is much smaller, there is no significant cancellation of errors, and it is perfectly natural to have an energy error smaller than the functional error. In fact, it is unavoidable once a is between 1 and 2.

In Fig. 3, we plot the ratio of the EDI to the ideal-DDE as a function of a, showing the divergence. Assuming linearity in the density and parabolic functionals, one finds this curve has shape $(1 + a)/(a - 1)$, plotted with dashes in the figure. (The ideal-DDE is proportional to $(a - 1)^2$, and the EDI is proportional to $(a^2 - 1)$.) Thus, for $a = 1.5$, the overestimate is a factor of 5. The EDI always overestimates, and the more accurate the density is, the greater the relative inaccuracy!

To show that none of these features are specific to this functional, in Table 3, we listed ideal- and pragmatic-DDEs of several popular approximate functionals (r^{2}SCAN , B3LYP[59], PBE[60], BLYP[61,62], and SVWN[63,64]) and two proxy benchmark functionals in Ref.[20,23,25,26] (r^{2}SCAN50[65] and LC-ωPBE[66]) on the H_2^+, ordered by their ideal-DDEs (CAM-B3LYP[67] and PBE0[68] on SI). With this measure, we can also say they are ordered in terms of the accuracy of their densities. We see that in every case, the size of the ideal-DDE is about 10 % larger than the corresponding absolute pragmatic-DDE value. Moreover, ordering with respect to the pragmatic-DDE is almost identical to that of the ideal-DDE (in Fig. S1 we also illustrate each of these functionals with curves analogous to Fig. 1, but keep in mind that the densities being scanned through as a function of a differ in every case).

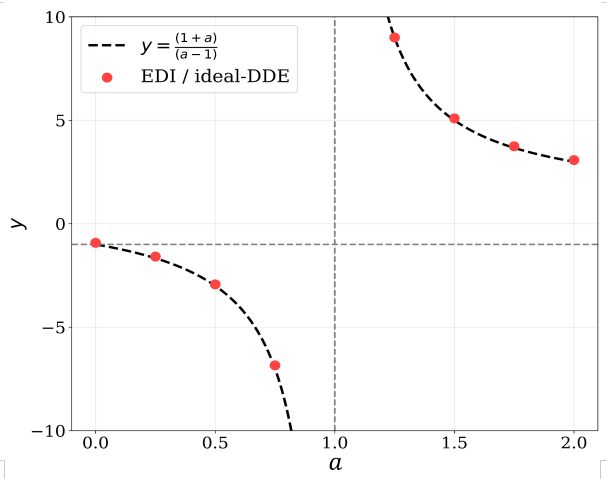

Figure 3: Ratio of the energetic density interpolator (EDI) to the ideal density-driven error (ideal-DDE) for r^{2}SCAN in H_2^+ at equilibrium. The red dots represent the calculated ratios evaluated on the self-consistent densities determined by the parameter a in Eq. 17, while the black dashed line represents the analytical prediction, $y = (1 + a)/(a - 1)$. The gray horizontal lines denote $y = -1$.

Table 3: Ideal- and pragmatic (prag.) density-driven error (DDE), functional error (FE), and total error (TE) in mH for H_2^+ at equilibrium. Results for total energy (top) and binding energy (bottom).

(mH)	type	r^{2}SCAN50	LC-ωPBE	SVWN	r^{2}SCAN	B3LYP	PBE	BLYP
				total energy				
DDE	ideal	0.16	0.62	0.66	0.68	0.91	1.25	1.62
	prag.	-0.15	-0.57	-0.63	-0.63	-0.84	-1.14	-1.47
FE		-2.49	-10.68	19.48	-4.97	-6.66	-5.52	-3.06
TE		-2.64	-11.25	18.85	-5.60	-7.50	-6.66	-4.53
				binding energy				
DDE	ideal	0.11	0.32	-0.37	0.49	0.51	0.60	0.88
	prag.	-0.11	-0.29	0.36	-0.45	-0.47	-0.56	-0.81
FE		-2.49	-4.69	-2.84	-4.97	-4.59	-6.11	-5.81
TE		-2.60	-4.98	-2.48	-5.43	-5.06	-6.67	-6.62

To show that the poor performance of the EDI is not somehow an artifact of our special family of densities, Table 4 presents a matrix of different approximate functionals applied to each other's self-consistent densities. The diagonals are the correct pragmatic-DDEs, and all others are (incorrect) estimates using Eq. 11. From their variation, it is clear that none are reliable, and r^{2}SCAN50 even producing incorrect signs, just as we found for $a > 1$ in our model example. For this system,

Table 4: Matrix of density-driven error (DDE) estimates (in mH) for H_2^+ at Equilibrium, calculated using energetic density interpolator (EDI, Eq. 11) across various density-functional combinations. The columns denote the functional used to generate density, while the rows denote the functional used for energy evaluation. Only diagonals (shaded) correspond to the correct pragmatic-DDEs. The range row indicates the spread of EDI values calculated by different functionals for a given density.

		density						
	(mH)	r²SCAN50	LC-ωPBE	SVWN	r²SCAN	B3LYP	PBE	BLYP
functional	r²SCAN50	-0.15	0.03	0.17	0.03	0.17	0.39	0.62
	LC-ωPBE	-0.40	-0.57	-0.29	-0.49	-0.50	-0.45	-0.30
	SVWN	-0.32	-0.35	-0.63	-0.33	-0.37	-0.24	-0.09
	r²SCAN	-0.46	-0.55	-0.32	-0.63	-0.57	-0.47	-0.38
	B3LYP	-0.53	-0.77	-0.58	-0.78	-0.84	-0.80	-0.75
	PBE	-0.63	-1.02	-0.75	-0.99	-1.09	-1.14	-1.09
	BLYP	-0.74	-1.20	-0.93	-1.22	-1.37	-1.42	-1.47
	range	0.59	1.23	1.10	1.25	1.54	1.81	2.09
	ideal-DDE	0.16	0.62	0.66	0.68	0.91	1.25	1.62

we conclude that the pragmatic-DDE is a good estimate of the ideal-DDE, but the EDI is highly inaccurate anywhere except at the self-consistent densities. This finding from a simple, exactly solvable model demonstrates the intrinsic limitation of applying the EDI to any non-self-consistent density: EDI is meaningful only at the self-consistent density of the functional from which it is derived. We will analyze this point in more detail in Sec. V.

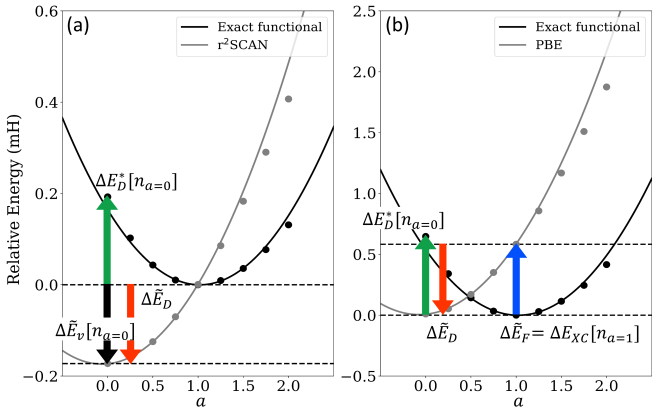

Figure 4: Two atypical cases: Exact (black) and DFT (gray, (a) r²SCAN and (b) PBE) energy functionals for the hydrogen atom, evaluated on the self-consistent densities of the functionals determined by the a in Eq. 17 The x-axis denotes the self-consistent density with respect to the parameter a in Eq. 17. Points are evaluations, and curves are parabolas that fit to the curvature at the minimum. The green (red) arrow shows the ideal (pragmatic) density-driven error, the blue arrow shows the functional error, and the black arrow denotes the total error.

Why did we not illustrate our points with the simplest of all one-electron systems, the H-atom? We did not choose this because the behavior of two of the most popular functionals (PBE and r²SCAN) is untypical in this case. However, both provide nice illustrations of DC-DFT principles. r²SCAN was chosen with the exact condition (norm) that, on the exact H-atom density, it yields the exact H atom energy of $-1/2$ (in Hartree).[69] Despite this, it makes a small error for the H atom, as its self-consistent density is not a simple exponential (see Fig. 4(a)), and it is about -0.173 mH lower in energy. True to its construction, that error vanishes at the exact density, so its error is entirely density-driven. The ideal-DDE agrees with the pragmatic-DDE to within about 10%. Thus, evaluation of r²SCAN on the exact density reduces the error to essentially zero, i.e., the posterchild of DC-DFT calculations, but hardly a typical case. On the other hand, the PBE functional shows a very different atypical behavior (see Fig. 4(b)). It was long ago shown that, *self-consistently*, PBE is essentially perfect for the H atom energy. So this *is* an example of functional error and pragmatic-DDE canceling exactly. Thus, here, swapping in the exact density only worsens the energy, and this is not a calculation that is improved. What DC-DFT does do is tell us that these perfect results is in fact an accidental cancellation of the two errors.

How does this ideal-DDE connect to (pragmatic) DC-DFT? The most appealing definitions are Eq. 7 for the functional error, and Eq. 15 for the ideal-DDE. But these two do not in general combine to yield the total error. The answer is simple. We continue to use the usual (pragmatic) DDE in DC-DFT (Eq. 10), as it is the only one we can calculate without recourse to the exact functional on approximate densities, which is rarely available. However, we consider it typically a good approximation to the ideal, and assume that is the case for most functionals in common use (i.e., those yielding useful accuracy for the problem at hand). Thus, for a given potential, different approximations will produce different self-consistent densities, with different DDEs. But if the curvature of the approximation is good, its pragmatic-DDE is an excellent estimate of its ideal-DDE[36], and it can be directly compared, as in Table 3.

Alternatively, there is a formulation of DC-DFT that uses the ideal-DDE, but combines it with the (equally impractical) functional error evaluated on the approximate density:

$$\Delta\widetilde{E}_v \approx \Delta E_{\mathrm{XC}}[\tilde{n}_v] + \Delta E_{\mathrm{D}}^*[\tilde{n}_v] \tag{18}$$

This formulation also yields the total error but from a slightly shifted perspective. Figure 5 shows the information in Fig. 1 more dynamically. Using a density closer to the exact density than the self-consistent one reduces total error (gray dots) by both lowering the ideal-DDE (green dots) and narrowing the gap between approximate and exact functionals at that density point (ΔE_{XC}, blue dots). This explanation describes how, from a total energy perspective, certain DC-DFT calculations can achieve smaller errors than functional error. The values are in Table 5. But this description is true when the approximate functional curve lies below the exact. If the curves have similar minima, or even if the approximate curve is located above the exact curve (situation like SVWN in Fig. S1), then as the density becomes more accurate (closer to $a = 1$), the total

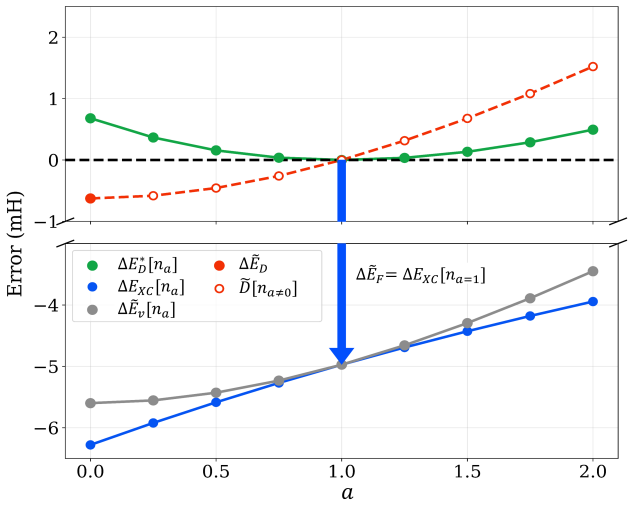

Figure 5: Error curves of H_2^+ at equilibrium for r^{2}SCAN. The x-axis denotes the self-consistent density with respect to the parameter a in Eq. 17. Ideal-DDE ($\Delta E^*_{\rm D}[n_a]$, green dots, Eq. 15), pragmatic-DDE ($\Delta\widetilde{E}_{\rm D}$, filled red dot, Eq. 10), EDI ($\widetilde{D}[n_{a\neq 0}]$, hollow red dots, Eq. 11), FE ($\Delta E_{\rm XC}[n_{a=1}]$, blue arrow, Eq. 7), XC energy deviation ($\Delta E_{\rm XC}[n_a]$, blue dots, Eq. 8), and TE ($\Delta\widetilde{E}_v[n_a]$, gray dots, Eq. 5). Even the density at $a=2$, where the ideal-DDE is same as self-consistent density ($a=0$), the total error is reduced because the reduction in $\Delta E_{\rm XC}$ is greater than the increase in $\Delta E^*_{\rm D}$.

error *increases*.

Table 5: Ideal density-driven error (ideal-DDE), exchange-correlation deviation ($\Delta E_{\rm XC}[n_a]$), and total error (TE) in mH of r^{2}SCAN evaluated on the self-consistent densities of the functionals determined by the parameter a in Eq. 17 for H_2^+ at equilibrium.

(mH)	value of a								
type	0.00	0.25	0.50	0.75	1.00	1.25	1.50	1.75	2.00
ideal-DDE	0.68	0.37	0.16	0.04	0.00	0.03	0.13	0.29	0.49
$\Delta E_{\rm XC}[n_a]$	-6.28	-5.92	-5.59	-5.27	-4.97	-4.69	-4.43	-4.18	-3.94
TE	-5.60	-5.56	-5.43	-5.23	-4.97	-4.66	-4.30	-3.89	-3.45

Our final discussion of energy curves for our one-electron cases fills in some details beyond Fig. 1. Figure 6 shows several different parabolas, and a solid purple line connecting their minima. The gray and the black are the original approximate ($a=0$) and exact functionals ($a=1$), respectively. The green parabola is the $a=1.5$ functional. We consider evaluating the original $a=0$ approximation on the $a=1.5$ density. This is a better density than the self-consistent density, and yields a smaller error than the functional error.

For each value of a, we plot the minimum energy of the corresponding functional $\widetilde{E}_a[n]$ (use XC functional as Eq. 17). These minimum points are connected by the solid purple line. We next draw a horizontal line to find the value of a where the purple line takes on the same value as the energy of the inconsistent evaluation $\widetilde{E}_{a=0}[\tilde{n}_{a=1.5}]$. This gives the minimizing density of the functional which self-consistently reproduces the energy of the inconsistent calculation, which in this case occurs at $a=0.22$–quite different from the $a=1.5$ density and still closer to the exact density ($a=1$) than the original approximate. The blue curve gives the energy of the $a=0.22$ functional.

We can generalize this analysis by taking any inconsistent evaluation $\widetilde{E}_{a=0}[\tilde{n}_a]$ and finding the value b such that the corresponding functional $\widetilde{E}_b[n]$ self-consistently produces the energy of the inconsistent evaluation, i.e.

$$\widetilde{E}_b[\tilde{n}_b] = \widetilde{E}_{a=0}[\tilde{n}_a] \tag{19}$$

A careful analysis of the condition Eq. 19, assuming curves are parabolic in a and densities are linear, yields the following equation for b:

$$b \simeq (a^2 - b^2)\frac{\Delta\widetilde{E}_{\rm D}}{\Delta E_{\rm XC}[\tilde{n}]} \tag{20}$$

With the approximations we have made, $\tilde{n}_b$ is the self-consistent density of the functional that reproduces the inconsistent result (ignoring any potential dependence of b in Eq. 20, which is likely to be small). This density is, in the sense of Eq. 2, the *true* density of the inconsistent calculation.

Note that b is typically small in this scenario (Table 6), because of the ratio of the energies. The dashed purple line in Figure 6 is the result of our formula Eq. 20, without the b^2 term. We assume that the above equation holds provided the minima of the curves lie approximately on a straight line.

In Table 6, we show various values of a; and the associated value of b found from Eq. 20. In every case, b differs substantially from a, i.e. the *true* density of the inconsistent evaluation $\widetilde{E}_{a=0}[\tilde{n}_a]$ is actually very far from $\tilde{n}_a$ itself. In fact, $\tilde{n}_b$ is likely to be quite close to the original self-consistent density $\tilde{n}_{a=0}$; but is more accurate, exhibiting a smaller ideal-DDE. The functional $\widetilde{E}_b[n]$ has both better energies and better densities than the original $\widetilde{E}_{a=0}[n]$, i.e. both its functional error and DDE are smaller than the original.

Table 6: The value of b according to a in Eq. 20 with r^{2}SCAN functional in the H_2^+ equilibrium.

	value of a								
type	0.00	0.25	0.50	0.75	1.00	1.25	1.50	1.75	2.00
b	0.0	0.01	0.02	0.06	0.10	0.15	0.22	0.30	0.38

Finally, we close by studying stretched H_2^+, the paradigm of self-interaction error[33]. We take the bond length to be 5 Å (Table 7), almost five times of equilibrium bond length. At this distance, any approximate functional with a self-interaction error makes a large error in the energy, because it is inaccurate

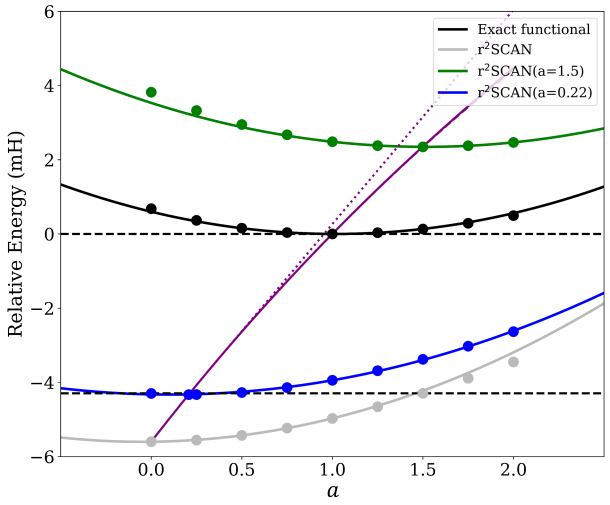

Figure 6: Energy curves same as in Fig. 1, but with the addition of the curve for a=1.5 in Eq. 17 (green) and energy error curve at a=1.5 estimated according to Eq. 20 (b = 0.22, blue). The x-axis denotes the self-consistent density with respect to the parameter a defined in Eq. 17. The purple solid line is the spline of the self-consistent energy error of the Eq. 17 functional according to the b value estimated through Eq. 20. The purple dotted line is the linear spline of the self-consistent energy error of the Eq. 17 functional based on the estimated b value obtained by removing the quadratic term of b from Eq. 20.

Table 7: Ideal and pragmatic density-driven error (DDE), functional error (FE), and total error (TE) in mH for (top) H_2^+ at 5Å and (middle) H atom. The bottom is the contribution to the binding energy.

(mH)	type	r²SCAN50	LC-ωPBE	SVWN	r²SCAN	B3LYP	PBE	BLYP
				H_2^+ at 5Å total energy				
DDE	ideal	4.60	3.46	5.11	5.56	2.42	1.16	2.08
	prag.	-4.66	-3.52	-5.18	-5.41	0.35	-1.18	-1.97
FE		-63.39	-63.52	-74.25	-75.18	-49.23	-31.69	-28.35
TE		-68.05	-67.04	-79.43	-80.60	-48.88	-32.87	-30.32
				H atom total energy				
DDE	ideal	0.04	0.30	1.02	0.19	0.40	0.65	0.74
	prag.	-0.04	-0.28	-0.99	-0.17	-0.37	-0.57	-0.66
FE		0.00	-5.99	22.32	0.00	-2.07	0.58	2.74
TE		-0.04	-6.27	21.33	-0.17	-2.44	0.01	2.09
				H_2^+ at 5Å binding energy				
DDE	ideal	4.55	3.16	4.09	5.37	2.02	0.52	1.34
	prag.	-4.62	-3.23	-4.19	-5.24	0.72	-0.60	-1.31
FE		-63.39	-57.53	-96.57	-75.18	-47.16	-32.28	-31.09
TE		-68.01	-60.77	-100.76	-80.42	-46.44	-32.88	-32.41

for the 1/2-electron densities localized on each proton. As the bond length is stretched to infinity, the energy does not approach that of a single H atom, as it should.

But this is *not* density-driven. This is plain to see in Table 7. Whether looking at the molecular energy or the contribution to the binding energy, the pragmatic-DDE is a small fraction of the functional error. The densities are reasonably accurate, and the error is functional-driven. Thus, while DC-DFT is a useful tool for studying systems with strong self-interaction errors, not all such errors are density-driven. This result is associated with the fact that DC-DFT, as described earlier in Fig. 5, causes error reduction not only through ideal-DDE but also through a decrease in $\Delta E_{\rm XC}$. Analogously, DC-DFT can be a useful tool for many other kinds of density errors, not just those caused by self-interaction. This distinction sometimes seems lost in the literature.

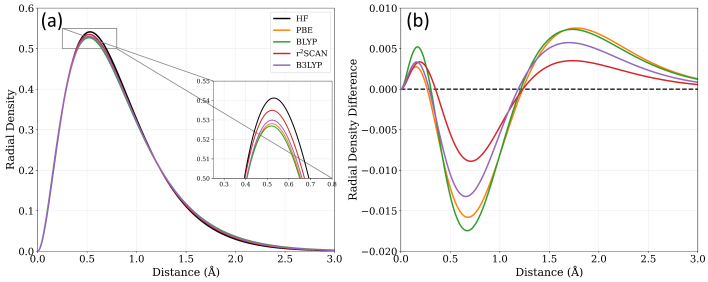

Figure 7: Radial densities (a) and radial density difference (b) of H atom for several functionals.

We close by discussing the relation between plots of density errors and DDEs. In Fig. 7, we show several densities and their errors for the H atom. The panel (a) shows how very close all of them are, and essentially indistinguishable by eye, except when zoomed in. In (b), we plot the errors in the densities, and looking at the minima in that figure, we might decide BLYP is least accurate, followed by PBE, B3LYP, and then r²SCAN . Consultation of Table 4 then shows that your intuition is good in this case, and DDEs (ideal or pragmatic) have the same ordering.

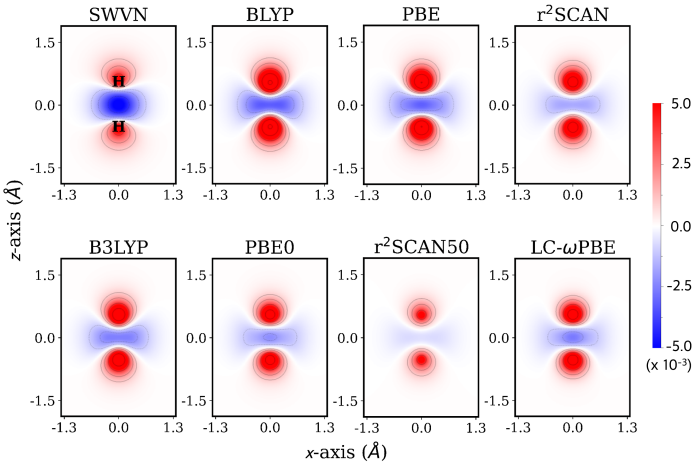

Figure 8: Contour map of density error $(n(\mathbf{r}) - n^{\rm HF}(\mathbf{r}))$ of H_2^+ at equilibrium for several functionals in xy-plane. Unit for density is $e/\text{Å}^3$.

But Fig. 8 shows the density errors for several functionals for H_2^+. By visual inspection, try ordering these 8 plots in order of their accuracy. Then compare your relative ordering with the results in Table 4. Chances are high you did not get them right. We have found no simple way to relate density error plots (or other metrics of density error) to those of DDE. We also point out that it is actually the difference between

DDEs that goes into DDEs for reaction differences, such as the binding energy of H_2^+. It is entirely unclear how to apply any metric of density error to the error in the difference of two densities with different external potentials.

IV2. Two-electron systems

To further illustrate the crucial distinctions between ideal- and pragmatic-DDE, we use the two-site Hubbard dimer model. The Hubbard dimer is a simplified model of a heteronuclear diatomic molecule, where electrons can hop between two sites and interact only when they doubly-occupy a site. The sites are subject to a potential difference Δv that establishes a site-occupation difference $n_2 - n_1$. For fixed hopping parameter and interaction strength t and U, the exact two-electron ground-state energy and density can be produced directly as a function of the potential. The associated KS quantities and inversion can be computed exactly, and all functionals can be plotted as functions of the density $E(n_1)$.

The density of the dimer is a number, with more accurate densities simply being close to that number. However, this is enough to define two qualitatively distinct types of errors for the density, and thus the logic of DC-DFT can be applied directly. The standard density functional approximations typically used in practice are generally not available for the dimer, but we demonstrate DC-DFT principles using unrestricted Hartree-Fock (UHF) and second-order density-functional perturbation theory (GL2)[70].

For the dimer it is simple to evaluate functionals using a density other than its corresponding self-consistent density. In fact, it is also possible to evaluate the corresponding self-consistent density associated to an inconsistent evaluation of density functional. For example, the GL2 total energy evaluated with the Hartree-Fock density $E^{\mathrm{GL2}}(n_1^{\mathrm{HF}}(\Delta v))$. The derivative with respect to Δv yields the associated density of all functionals, including the self-consistent density of the *inconsistent* evaluation, as discussed in Sec. II2, which is plotted in green in Fig. 9.

In the strongly-correlated regime ($\Delta v < U$), the UHF density is closer to the exact, when compared to the GL2 density. However, UHF is a poorer approximation of the energy, and thus provides a range of parameters where DC-DFT can be demonstrated. The density associated to the inconsistent evaluation of the GL2 functional with the UHF density, the green curve of Fig. 9, provides a slight improvement over the GL2 self-consistent density.

Figure 10 is a generalization of Fig. 1, and the exact ground-state and HF density functionals are evaluated with a self-consistent density $n_{1,a}(\Delta v)$, where $0 \leq a \leq 1$ interpolates between pure HF exchange ($a = 0$) and exact total XC ($a = 1$).

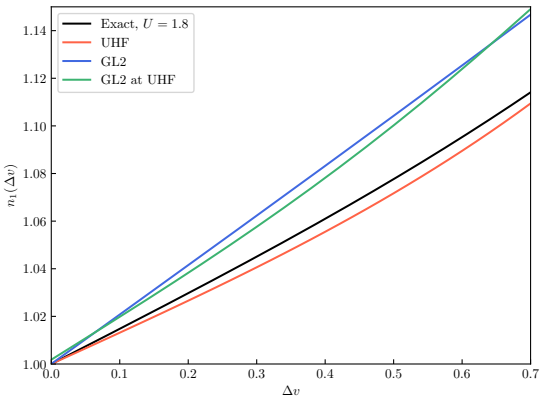

Figure 9: Exact (black), unrestricted Hartree-Fock (red), second-order Görling-Levy perturbation theory (blue), and inconsistent evaluation of GL2 density functional with UHF density (green).

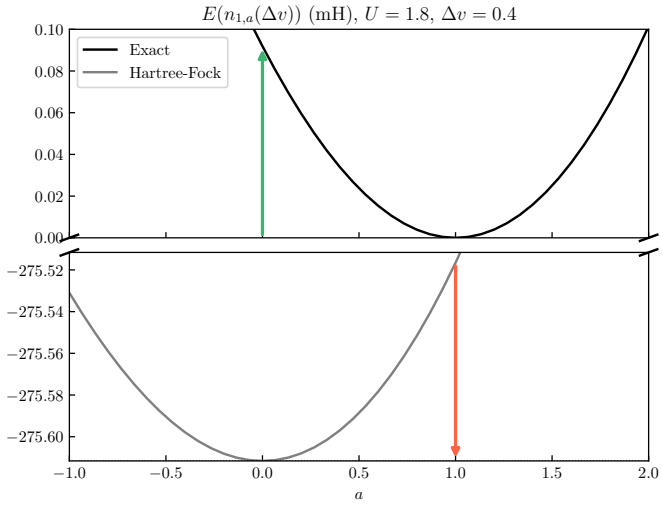

Figure 10: Exact (black) and UHF (gray) density functionals evaluated at density $n_{1,a}(\Delta v)$, which interpolates between Hartree-Fock ($a = 0$) and exact ($a = 1$).The green and red are ideal and pragmatic density-driven errors respectively. Both curves are shifted by their respective "atomic-limit" values, where hopping $t \to 0$.

In this interacting case, the pragmatic- and ideal-DDEs are roughly equal and opposite. This trend continues over the range of plotted Δv values. From Fig. 11, at $\Delta v = 0.4$ the pragmatic-DDE is comparable in magnitude to the ideal. As Δv increases, the dimer becomes weakly correlated, and for all plotted parameters, minus the pragmatic-DDE remains within ± 10 %.

Figure 12 is analogous to Fig. 6. We observe that the self-consistent GL2 density is further from the exact ($a \approx 0.7$), and the total error in the energy is roughly -70 mH. The Hartree-Fock provides a poor approximation to the energy, but the self-consistent UHF density is closer to the exact. Thus, the density correction provided by the UHF density

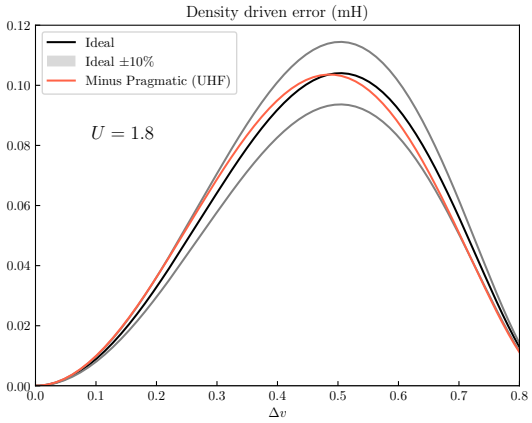

Figure 11: Ideal (black) and minus the pragmatic (red) density-driven errors (DDE) plotted for a range of external potentials. The shaded regions are ±10 % the ideal-DDE. Minus the pragmatic-DDE is within the shaded regions for many values of strongly-correlated $\Delta v < U$.

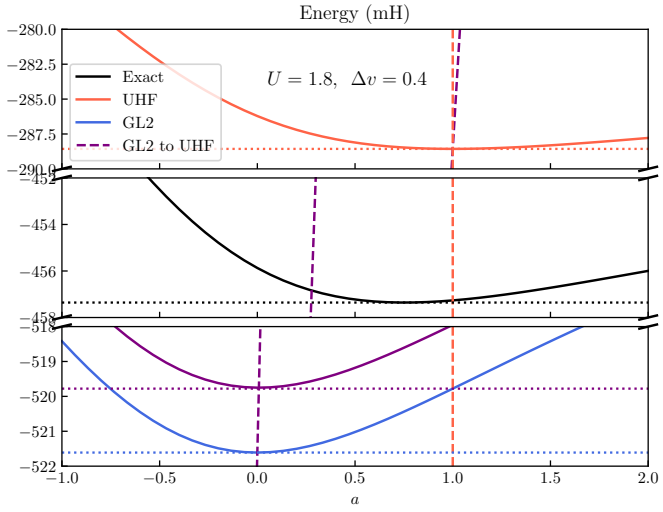

Figure 12: Exact (black), unrestricted Hartree-Fock (red), and second-order density-functional perturbation theory (blue) energies, density-corrected (purple). Here self-consistent densities are denoted with dashed vertical lines. The density-corrected energy (dotted purple) is the improved prediction of the energy by substituting the Hartree-Fock density into the GL2 functional.

reduces the total error slightly by reducing the ideal-DDE. We plot exact and approximate density functionals evaluated with $n_{1,a}(\Delta v)$, which interpolates between GL2 ($a = 0$) and HF ($a = 1$). The dashed purple line connects the GL2 and UHF minima, unlike Fig. 6, and the purple dotted line denotes the density-corrected energy. The dashed and dotted purple lines intersect at $a \approx 0.08$, which is approximately the minimum of the true density-corrected density-functional corresponding to the inconsistent GL2 evaluation.

IV3. Summary of model systems

This survey has produced several key concepts in DC-DFT. First, the ideal-DDE is well-defined for every system and depends only on the approximate density, not on an approximate energy functional. Second, the pragmatic-DDE uses the approximate functional to estimate the ideal, typically producing about a 10 % underestimate (and the opposite sign). We found no cases where it was not a good estimate. Third, the use of any density other than the self-consistent density in the EDI almost always fails to give a good estimate of the DDE (ideal or pragmatic). Collectively, these results highlight that the ideal-DDE serves as the rigorous theoretical standard but is primarily of conceptual value, as evaluating it for realistic systems requires the unavailable exact functional.

V. Practicalities

The previous section was written to demonstrate basic principles of DDEs. But it was confined to either one-electron systems or model two-electron systems. Now we study the realistic cases that have caused controversy in the literature, using the insight garnered from the previous sections.

Why are there still questions about how DC-DFT produces such improvements? In practice, the HF density often serves as a practical tool for density-correction. Several studies in the literature, using other measures of density error, have suggested that HF densities can, in certain cases, deviate more than self-consistent DFT densities according to those measures.[23,25,71] As mentioned above, and studied below, the difficulty lies in relating those measures to DDEs, especially for chemical energy differences. We have found no simple relationship between such measures and DDEs.

A second issue is how to measure the DDE of an HF-DFT calculation (i.e., an approximate density functional evaluated on the HF density). An essential problem is that we do not know the exact density of such a calculation. Its density is neither the HF density nor the self-consistent density of the approximate functional. It is given by Eq. 13, but we have no practical means to calculate this. The results of Sec. IV yield a better density than the self-consistent one in that specific case, butthe methodology only works in toy-model cases such as ours. Then, even if we had this density, we cannot calculate the ideal-DDE without the exact functional, nor can we calculate the pragmatic-DDE without having the pure density functional for which this density is a self-consistent minimum. As discussed below, some recent works have employed the EDI as an approximate estimator of pragmatic-DDE, although our analysis indicates that it is not directly related to the rigorous DDE definition.

Practically, the question then becomes how one might proceed in the absence of exact DDEs. Density sensitivity provides a practical heuristic for identifying cases where density correction—whether implemented through HF-DFT or another DC-DFT variant—can be beneficial. When the density sensitivity is large (with a threshold that depends on system size and type), one may reasonably expect a meaningful energetic improvement over the self-consistent result. Thus, while not universal, density sensitivity remains a useful indicator of when density correction is likely to be advantageous.

V1. Proxy benchmark densities, and their pitfalls

For many systems, it can be extremely challenging to evaluate even the pragmatic-DDE. First, one needs a reliable calculational method that produces highly accurate densities. Then one must perform a Kohn-Sham inversion, i.e., find the KS potential whose ground-state density is the accurate density. This problem has a long and difficult history.[7,10,72–80] Finally, armed with the KS orbitals, one can calculate the approximate functional's energy on the exact density. As this is often not practical for systems of chemical interest, ways have been found to bypass these steps.

Recent literature has used proxy benchmark densities as surrogates for the (unknown) exact density when evaluating DDEs for molecules. These are self-consistent densities from other density functional approximations that are treated as if they were the exact density. For example, Kaplan and others[20] present an analysis of error decomposition for barrier heights, evaluated against three such proxy benchmark densities: SX-0.5, SCAN-FLOSIC, and LC-ωPBE. The authors estimate pragmatic-DDE using these proxy benchmark densities in place of the exact density $n_v(\mathbf{r})$, see Eq. 10:

$$\widetilde{\mathcal{E}}_{\mathrm{D}}[\tilde{n}; n_{proxy}] = \widetilde{E}_v[\tilde{n}] - \widetilde{E}_v[n_{proxy}]. \tag{21}$$

Here, we will refer to the quantity in Eq. 21 as the proxy-DDE. If the exact density is used in place of the proxy benchmark density, this becomes the pragmatic-DDE. Each of these proxy benchmark methods is an approximate KS-DFT method, and so yields both a density and its corresponding orbitals, thereby making evaluation of $\widetilde{E}[n_{proxy}]$ simple. But, as discussed earlier, pragmatic-DDEs are typically much smaller than functional errors, and one needs to be able to rank self-consistent densities of different functionals. Thus a proxy benchmark method needs to be precise enough to distinguish small differences among already small numbers.

In the case that $n_{proxy}(\mathbf{r})$ is extremely close to the exact density, $\widetilde{\mathcal{E}}_{\mathrm{D}}$ is a good estimate of the pragmatic-DDE. Without more accurate benchmark densities, it is impossible to determine the efficacy of a proxy benchmark densities (i.e., quantify how close the proxy benchmark is to the exact density). However, if multiple different proxy benchmarks are suggested, then some tests of internal consistency can be performed. First, when evaluating the pragmatic-DDEs of a set of functionals using the proxy benchmark densities, the ranking of those functionals (i.e., which has the lowest proxy-DDE) should be consistent among all the proxy benchmark densities used. Second, for the proxy benchmarks to be useful, the spread among the proxy-DDEs should be small relative to the pragmatic-DDE itself. If their spread is a significant fraction of the pragmatic-DDE, this would render the proxy benchmark densities dubious as useful estimators.

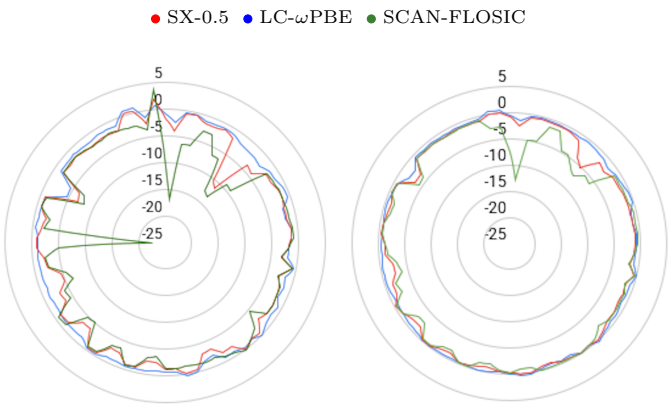

(a) PBE **(b)** SCAN

Figure 13: Reaction-by-reaction breakdown BH76. Proxy-DDEs for PBE and SCAN functionals using the three proxy benchmark densities (in kcal/mol) are plotted on the radial coordinate. The angular coordinate corresponds to the reaction index. In some (density-sensitive) cases, the proxy benchmarks disagree by more than 20 kcal/mol. The spread of proxy-DDEs across the proxy benchmarks is sensitive to both the functional used, and the system in question. Three proxy-DDEs results are from Ref.[20].

Here we analyze the results reported in Ref.[20] for the three proxy benchmark densities suggested there, for the proxy-DDEs of the BH76 set of barrier heights. We find that in over a third of cases, the proxy benchmarks disagree on which functional has the lowest proxy-DDE (see Table S7). Kaplan et al.[20] point to the consistency of the proxy-DDE averaged over the reactions of the three proxy benchmarks, but this ignores their deviations for each reaction. We stress the importance of examining the proxy benchmarks on a case-by-case basis, revealing significant inconsistencies which can be obscured by averaging. Figure 13 shows the variations in proxy-DDE for their three different proxy benchmark densities and two different functionals, PBE and SCAN[81] across the systems of BH76. The figure should already be alarming, showing some extreme variations, especially for SCAN-FLOSIC.

For simplicity, we choose the average of the three proxy-DDEs (evaluated on the three densities) as the best estimate of the pragmatic-DDE, and the spread (max minus min) as

an estimate of its uncertainty (reporting the results for all 76 reactions in the Table S7). However, we emphasize that these "proxy benchmark densities" (SX-0.5, LC-ωPBE, and SCAN-FLOSIC) have been proposed [20,23] as three independent approximations to a high-quality density, and the fact that they differ by several mH means that averaging any subset of them does not yield a more meaningful benchmark; rather, the spread itself reflects the intrinsic ambiguity in defining a "proxy benchmark density". Table 8 lists results averaged over BH76 of proxy-DDE using each of the three proxy benchmark densities and the spread. In fact, the spreads are significant on the scale of the proxy-DDEs themselves. Furthermore, examining the proxy-DDEs of the RKT10 transition state barrier (Table 9), for which a high-accuracy benchmark density is available, we see that the proxy benchmarks are essentially useless, as their spread is larger than the known pragmatic-DDE itself. Finally, analyzing the density sensitivities of the BH76 systems (calculated in Ref. [21]) shows that the reactions with the widest range of proxy-DDEs across the proxy benchmarks are generally highly density sensitive. We present some of the worst cases in Table 10; and it is precisely in these cases that the application of the HF density tends to cure the errors. [21]

Table 8: Uncertainties due to proxy benchmark densities on BH76 dataset, calculated from data presented in the SI of Ref. [20]: Mean and mean range of proxy-DDE calculated with three different proxy benchmark densities, averaged over BH76. The deviation among the proxy benchmark densities is comparable to the proxy-DDEs themselves.

functional	avg. DDE (kcal/mol)	avg. range (kcal/mol
PBE	-2.37	2.69
B3LYP	-0.76	0.63
SCAN	-1.24	1.56
BLYP	-2.28	1.09

Table 9: Proxy-DDEs (kcal/mol) for the RKT10 ($H\cdots H\cdots F$) forward and reverse barriers using the three proxy benchmark densities, and pragmatic-DDE by using CCSD(T) benchmark density. The proxy-DDEs deviate significantly from the pragmatic-DDE (by at least 1 kcal/mol) for each functional. Proxy-DDEs are from Ref. [20], pragmatic-DDEs are from Ref. [23].

functional (barrier direction)	LC-ωPBE	SX-0.5	SCAN-FLOSIC	CCSD(T)
PBE (forward)	-1.31	-4.87	-6.44	-2.20
SCAN (forward)	-0.29	-2.52	-3.80	-1.00
PBE (reverse)	-1.11	-4.57	-5.45	-2.30
SCAN (reverse)	-0.22	-2.31	-3.15	-1.20

V2. Unreliability of energetic density interpolator

We next apply the theoretical framework developed above to recent HF-DFT studies that have generated some ambiguity regarding interpretation. We focus primarily on barrier heights, and in particular on $H_2 + F \rightarrow H\cdots H\cdots F$ and an analog, as these have known densities and KS inversions. This system was studied in the context of DC-DFT by Kanungo et al. [23], wherein the EDI is used extensively. In this section, unless otherwise noted, we used CCSD(T) [42,82,83] energy as $E_v[n_v]$ while used KS inverted CCSD density as $n_v(\mathbf{r})$ to get pragmatic-DDE by using KS-pies [84] code. Although CCSD(T) density should have been used for better accuracy, it was not done due to the significant computational cost of generating the density (Table S8 compares the total energy differences between CCSD and CCSD(T) densities for several atoms and anions and functionals, with differences less than 1 kcal/mol).

Table 10: Average and range of three (SX-0.5, LC-ωPBE, and SCAN-FLOSIC) proxy-DDEs [20] (kcal/mol) of PBE and SCAN (Eq. 21) for four BH76 systems with significant disagreement between the proxy benchmark densities. Proxy-DDEs are from Ref. [20].

system	PBE (Avg / Range)	SCAN (Avg / Range)
$OH + N_2 \rightarrow N_2OH$ (ts)	−7.7 / 14.5	−5.5 / 11.2
$H + F_2 \rightarrow HF_2$ (ts)	−8.3 / 11.0	−3.6 / 5.9
$HF + F \rightarrow HF_2$ (ts)	−8.9 / 11.5	−4.4 / 6.7
$H_2 + PH_2 \rightarrow$ RKT12	−8.2 / 21.6	−0.6 / 0.2

Table 11: Matrix of density-driven error (DDE) estimates (in kcal/mol) same as Table 4, but for the $H_2 + F \rightarrow H\cdots H\cdots F$ reaction (transition state, reactant, and barrier height), calculated using the energetic density interpolator (EDI, Eq. 11) across various density-functional combinations. The columns denote the functional used to generate the density, while the rows denote the functional used for energy evaluation. Only the diagonal values (shaded green) correspond to the correct pragmatic-DDEs. The range row indicates the spread of EDI values calculated by different functionals for a given density. Bold numbers indicate the density yielding the smallest EDI for each functional.

		density						
	(kcal/mol)	SVWN	PBE	r^{2}SCAN	B3LYP	PBE0	r^{2}SCAN50	LC-ωPBE
		transition state						
functional	SVWN	-9.17	-7.10	-4.36	-5.36	**-3.84**	4.42	-4.53
	PBE	**-2.41**	-4.45	-3.14	-3.64	-2.79	3.33	-2.89
	r^{2}SCAN	2.77	**-0.51**	-1.81	-1.23	-1.42	1.48	-0.83
	B3LYP	**1.40**	-1.43	-1.66	-2.24	-1.80	1.94	-1.74
	PBE0	3.85	**0.43**	-0.85	-0.79	-1.23	1.10	-0.66
	r^{2}SCAN50	11.52	6.39	1.74	2.61	**0.72**	-1.72	2.07
	LC-ωPBE	2.24	**-0.50**	-1.08	-1.56	-1.50	1.48	-2.07
	range	20.69	13.49	6.1	7.97	4.56	6.14	6.60
		reactant						
functional	SVWN	-4.14	-2.37	**-0.66**	-2.19	-1.25	1.80	-2.24
	PBE	**0.00**	-1.76	-0.84	-1.59	-1.15	1.18	-1.51
	r^{2}SCAN	2.89	0.37	-0.56	**0.02**	-0.36	0.21	0.10
	B3LYP	**0.66**	-1.11	-0.70	-1.29	-0.90	0.91	-1.04
	PBE0	2.42	0.17	-0.26	-0.07	-0.46	0.46	**0.00**
	r^{2}SCAN50	5.49	2.52	0.26	1.70	**0.40**	-0.54	1.82
	LC-ωPBE	**0.46**	-1.17	-0.78	-1.19	-0.99	0.88	-1.44
	range	9.63	4.89	1.10	3.89	1.65	2.34	4.06
		barrier height						
functional	SVWN	-5.03	-4.73	-3.70	-3.17	-2.59	2.62	**-2.29**
	PBE	-2.41	-2.69	-2.30	-2.05	-1.64	2.15	**-1.38**
	r^{2}SCAN	**-0.12**	-0.88	-1.25	-1.25	-1.06	1.27	-0.93
	B3LYP	0.74	**-0.32**	-0.96	-0.95	-0.90	1.03	-0.70
	PBE0	1.43	**0.26**	-0.59	-0.72	-0.77	0.64	-0.66
	r^{2}SCAN50	6.03	3.87	1.48	0.91	0.32	-1.18	**0.25**
	LC-ωPBE	1.78	0.67	**-0.30**	-0.37	-0.51	0.60	-0.63
	range	11.06	8.60	5.18	4.08	2.91	3.80	2.54

Begin with the unreliability of the EDI (Eq. 11) when applied inconsistently. Table 11 shows precisely the same patterns as we found in Table 4. In many cases, applying the EDI to a density produced by a different functional leads to large

deviations. To emphasize how dependent the numbers are on the choice of functional, we report the range (max minus min) of results for each given density; and we find that these errors are significant on the scale of the pragmatic-DDEs themselves. We also boldface the smallest EDI in each row. Again, we find no relation between the EDI and the true pragmatic-DDEs.

Table 12: Same as Table 11, but with $H_2 + Cl \rightarrow H\cdots H\cdots Cl$.

	(kcal/mol)	SVWN	PBE	r^{2}SCAN	B3LYP	PBE0	r^{2}SCAN50	LC-ωPBE
					density			
					transition state			
functional	SVWN	-5.60	-3.92	**-0.88**	-3.32	-1.89	3.11	-1.74
	PBE	**-0.74**	-2.39	-1.08	-1.99	-1.53	1.84	-0.78
	r^{2}SCAN	3.40	0.11	-1.19	**0.08**	-0.73	0.29	0.46
	B3LYP	**0.23**	-1.60	-0.72	-2.01	-1.38	1.17	-0.81
	PBE0	2.78	**-0.02**	-0.43	-0.26	-0.89	0.48	0.07
	r^{2}SCAN50	7.23	2.92	0.11	1.79	**-0.05**	-1.42	1.22
	LC-ωPBE	1.44	-0.73	-0.78	-1.22	-1.49	**0.13**	-2.47
	range	12.83	6.84	1.30	5.11	1.84	4.53	3.69
					reactant			
functional	SVWN	-4.75	-3.22	**-0.21**	-3.1	-1.57	2.35	-2.42
	PBE	**-0.43**	-1.94	-0.67	-1.74	-1.31	1.19	-1.30
	r^{2}SCAN	3.61	0.41	-0.87	0.36	-0.53	**-0.13**	0.15
	B3LYP	**-0.24**	-1.70	-0.65	-1.90	-1.32	0.82	-1.15
	PBE0	2.53	-0.02	-0.31	-0.08	-0.66	0.35	**0.01**
	r^{2}SCAN50	6.28	2.30	-0.18	1.83	**0.10**	-0.93	1.61
	LC-ωPBE	**0.46**	-1.22	-0.88	-1.14	-1.23	0.58	-1.91
	range	11.03	5.52	0.70	4.93	1.67	3.28	4.03
					barrier height			
functional	SVWN	-0.85	-0.70	-0.67	**-0.22**	-0.32	0.76	0.68
	PBE	-0.31	-0.45	-0.41	-0.25	**-0.22**	0.65	0.52
	r^{2}SCAN	-0.21	-0.30	-0.32	-0.28	**-0.20**	0.42	0.31
	B3LYP	0.47	0.10	-0.07	-0.11	**-0.06**	0.35	0.34
	PBE0	0.25	**0.00**	-0.12	-0.18	-0.23	0.13	0.06
	r^{2}SCAN50	0.95	0.62	0.29	**-0.04**	-0.15	-0.49	-0.39
	LC-ωPBE	0.98	0.49	0.10	**-0.08**	-0.26	-0.45	-0.56
	range	1.83	1.32	0.96	0.24	0.26	1.25	1.24

To ensure these are not accidental results of a given reaction, we repeat the process with $H_2 + Cl \rightarrow H\cdots H\cdots Cl$ in Table 12. If you look at the values column-wise, we can see how different approximate functions evaluate the energy differently for the same density. Again, we find no EDI for any approximate functional yields accurate pragmatic-DDE. Also, we did not observe consistent predictive behavior of the EDI for the pragmatic-DDE. Even SVWN density has the smallest EDI among the 7 densities in some cases. This behavior occurs because each approximation samples and weights electron density differently across space, meaning that even visually similar densities can yield markedly different energies depending on the approximation employed. Therefore, it is not possible to infer density similarity from energy agreement, nor to evaluate the quality of a density based solely on its spatial resemblance to a benchmark. Discussing density quality outside the context of its self-consistent functional is meaningless. Conventional density metrics based solely on spatial similarity are physically unfounded and potentially misleading for assessing density accuracy.

Figure 14 is a density error contour map of the $H\cdots H\cdots F$ transition state in the xy plane, while Fig. 15 repeats this for Cl in place of F. Visually, the HF, SVWN, PBE, r^{2}SCAN , and B3LYP densities appear to be more different from the benchmark, while the densities of PBE0, r^{2}SCAN50, and LC-ωPBE appear to be less different. In Refs.[23,54], and[71], they insist that the HF density is inaccurate because it looks spatially

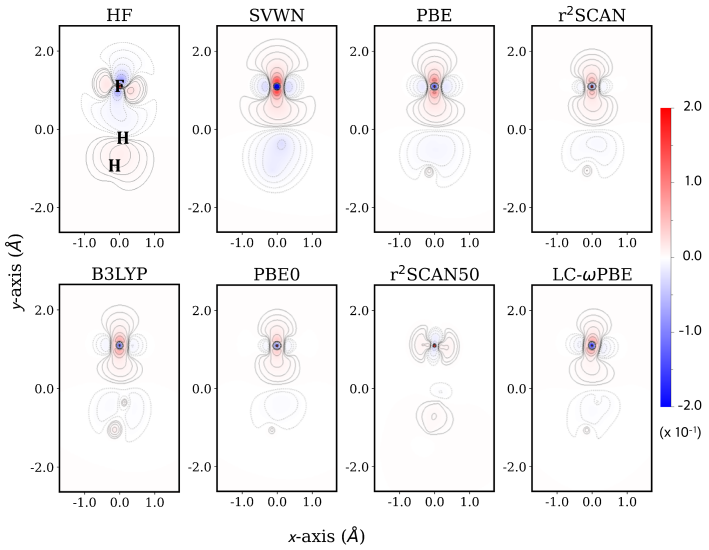

Figure 14: Contour maps of density errors (e/Å^3) for the $H\cdots H\cdots F$ transition state, using CCSD as the benchmark. On this scale, CCSD and CCSD(T) appear identical (see Fig. S6).

different from the density of the coupled-cluster methods. However, as noted in Ref.[50], spatial differences in electron density do not directly imply improved accuracy, nor is the relationship between density errors and energy errors straightforward.

V3. Proxy errors related to EDI errors

We have already seen that proxy benchmark densities introduced in the literature produce such a range of values that it undermines their credibility as a proxy of accurate density. We have also just documented how poorly the EDI performs when applied to any density other than its own self-consistent density, when it yields the pragmatic-DDE. In this section, we show that these two phenomena are intrinsically linked.

Table 13: Relationship between proxy-DDE ($\widetilde{\mathcal{E}}_{\rm D}$), EDI ($\widetilde{D}$), and pragmatic-DDE ($\Delta\widetilde{E}_{\rm D}$), shown numerically for the forward RKT10 barrier height ($H_2 + F \rightarrow H\cdots H\cdots F$). Unit in kcal/mol.

functional	n_{proxy}	$\widetilde{D}[n_{proxy}]$	$\widetilde{\mathcal{E}}_{\rm D}[\tilde{n};n_{proxy}]$	$\Delta\widetilde{E}_{\rm D}$
PBE	LC-ωPBE	-1.38	-1.31*	-2.69
PBE	r^{2}SCAN50	2.15	-4.85	-2.69
SCAN	LC-ωPBE	-0.95	-0.29*	-1.24
SCAN	r^{2}SCAN50	1.28	-2.53	-1.24

* $\widetilde{\mathcal{E}}_{\rm D}$ values for LC-ωPBE were obtained from Ref.[20].

The proxy-DDE ($\widetilde{\mathcal{E}}_{\rm D}$) and the EDI ($\widetilde{D}$) follow an exact relationship. For a given proxy benchmark density, and approximate functional, adding together Eqs. 11 and 21 gives:

$$\widetilde{\mathcal{E}}_{\rm D}[\tilde{n};n_{proxy}] = \Delta\widetilde{E}_{\rm D} - \widetilde{D}[n_{proxy}] \qquad (22)$$

This is illustrated in Table 13. But the interpretation is very interesting. In particular, we see that the error made by $\tilde{\mathcal{E}}_D$

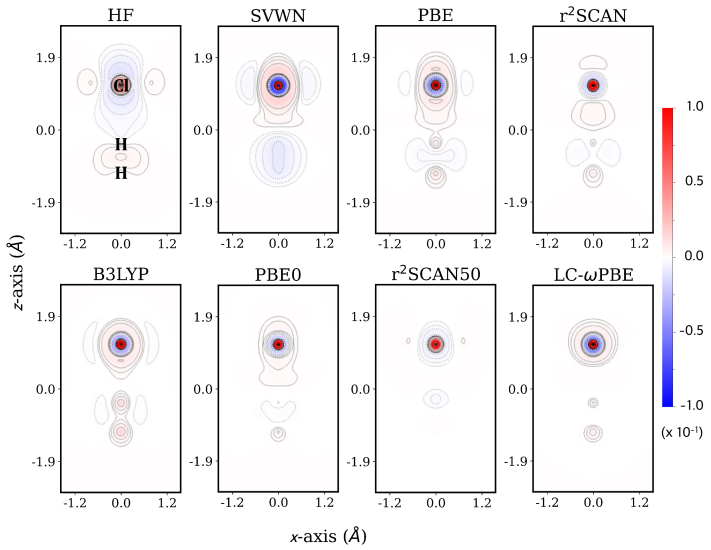

Figure 15: Same as Fig. 14, with F replaced by Cl (see Fig. S7).

in predicting the pragmatic-DDE is exactly the EDI of the proxy density. If the proxy benchmark density was close to the exact density, $\widetilde{D}[n_{proxy}]$ would be much smaller than pragmatic-DDE, and $\widetilde{\mathcal{E}}_{\mathrm{D}}$ would be close to the pragmatic-DDE. We clearly see that this is not true for the crucial case of $H_2 + F \rightarrow H\cdots H\cdots F$, a case where a sufficiently accurate density was found and inversion could be done. In *every* case, the proxy benchmark density yields a terrible estimate of the pragmatic-DDE. We can now relate the failure of proxy benchmarks to the overestimates of EDI.

Suppose the second term of the right-hand side in Eq. 22 was the ideal-DDE rather than the EDI. Then, if the proxy benchmark density was sufficiently close to the exact density, the error between the proxy-DDE and the pragmatic-DDE would vanish quadratically (since the ideal-DDE is quadratic in the density difference[36]). Then, $\widetilde{\mathcal{E}}_{\mathrm{D}}$ might be a good estimate of the pragmatic-DDE (at least, the error vanishes quickly as the proxy benchmark density becomes increasingly accurate). However, this is *not* the case. Instead, the second term in Eq. 22 is the EDI, which based on our analysis in the previous sections, is *linear* in the density difference rather than quadratic, and much larger than the pragmatic-DDE. Thus, the proxy-DDE inherits the inaccuracy of the EDI–and its error shrinks only linearly as the proxy benchmark density approaches the exact density. The proxy benchmark density would have to be extremely close to the exact density to make this error negligible, and none of the proxy benchmark densities suggested in recent literature meet this criterion.

V4. Analysis in terms of total energies

In this last section, we work backwards and decompose the errors in chemical reaction energies into their total energy components, such as the transition state and the reactants in the case of a barrier height. Although density functional approximations often yield large absolute errors in total energies due to intrinsic limitations when their functional forms are applied to core electrons, they are nonetheless highly effective in predicting relative quantities such as reaction energies and barriers. The errors in total energies are often much larger than the energy difference itself, and vary enormously among different approximate functionals. The reliability for energy differences largely stems from a systematic cancellation of functional errors: when the energetic errors of the reactants and products are of comparable magnitude, their difference–the relative energy–remains accurate even if the respective errors are significant.

As stated repeatedly above, unfortunately, we cannot directly measure the HF-DFT's DDE, or even have a good estimate. What we can do is calculate the pragmatic-DDE of self-consistent functionals when we can calculate accurate densities and perform sufficiently accurate KS-inversions. Figure 16 presents the distribution of the ratio of the product pragmatic-DDE divided by the reactant pragmatic-DDE for 103 benchmark reactions. (See Table S9 for a complete list of reactions selected based on whether they were small enough to allow CCSD density calculations in the GMTKN55 and Bauzá30[85] datasets.) If the pragmatic-DDE of the reactant and product are similar, their values in the energy difference will cancel each other out and will not affect the overall error. In the density-insensitive case, the distribution of ratios is relatively clustered around 1. However, in the density-sensitive case, the ratios are distributed far from 1. It is clear that the difference in error between reactant and product mentioned affects pragmatic-DDE as in Table 11. A few outliers far from 1 in density-insensitive cases may look quite strange, but this occurs only because the reactant pragmatic-DDE in the denominator is very small (see the number next to the marker).

V5. Relationships between density-driven errors and standard metrics of density errors

Quantitatively assessing the accuracy of an electron density is inherently challenging. The DFT literature is full of density error plots and many different metrics to measure density differences. In fact, one can devise infinitely many such measures, and different ones are used to make different points. Some show self-consistent densities to be preferable, others find HF densities better.

An important point to note is that, for spatially open-shell cases, there is freedom in the orientation of the orbitals, which must be accounted for when calculating the error. This occurs for some commonly used metrics, such as the L_2 norm or differences in Coulomb self-energy. For systems with degenerate electronic configurations, the orientation and occupation

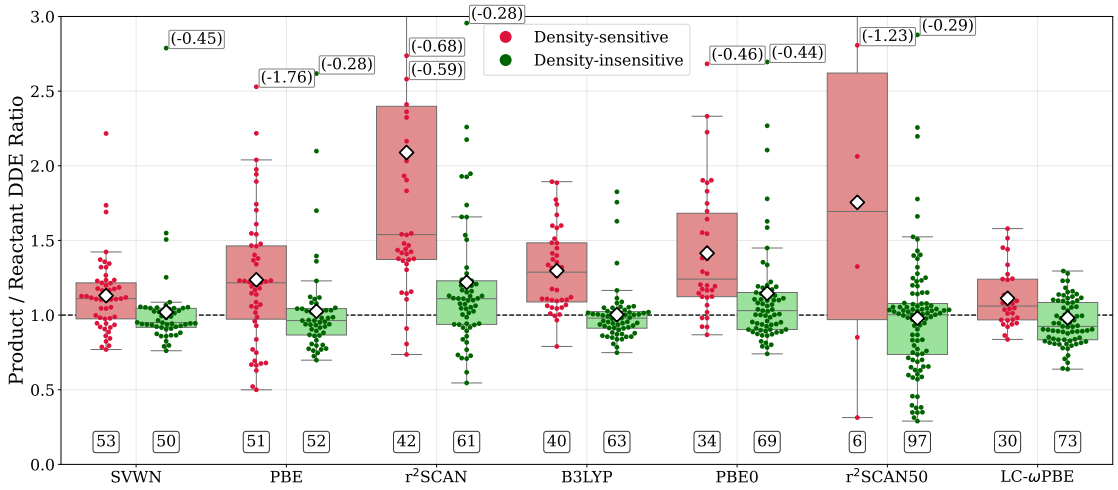

Figure 16: Distributions of the ratio of pragmatic density-driven error (pragmatic-DDE) between product and reactant for 103 benchmark reaction energies (see Table S9 for the full list). Reactions are categorized as density-sensitive (red) or density-insensitive (green). The number below each box indicates the number of reactions included in that category. White diamond markers denote the mean pragmatic-DDE ratio within each box. For cases where the ratio exceeds 2.5, the corresponding value in parentheses indicates the pragmatic-DDE of the reactant (in kcal/mol). In density-insensitive reactions, the pragmatic-DDE ratio is generally clustered around 1, indicating similar pragmatic-DDE contributions from both reactants and products. In contrast, density-sensitive reactions exhibit larger deviations from 1, suggesting significant differences in pragmatic-DDE between reactant and product. These results support the view that pragmatic-DDE contributes to energy errors primarily in density-sensitive cases, highlighting a link between pragmatic-DDE magnitude and density sensitivity.

of atomic or molecular orbitals can vary arbitrarily without affecting observable properties such as energies. Figure 17 illustrates this point: Due to the degeneracy of the O atom's $2p$ orbitals, electron densities computed using the same functional (e.g., PBE) may differ in shape. In such cases, direct comparison of real-space densities becomes unreliable, even when the densities are obtained using the identical method, unless this ambiguity is removed. As a result, spatial features of the electron density may differ in ways that are not physically significant, thereby confounding numerical comparisons. This degeneracy-related variability in real-space density distributions can lead to misleading conclusions when comparing electron densities across different calculations or methods.

To avoid spatial ambiguities—such as the orbital occupation variability illustrated in Fig. 17—a subset of 36 reactions was selected from the 103 benchmark reactions in Table S9 (see the reaction index that marked with an asterisk in Table S9). Only reactions involving closed-shell or non-degenerate open-shell species were included, allowing for reliable correlation analysis between pragmatic-DDE and real-space density metrics. This subset avoids artifacts arising from arbitrary orbital occupations in degenerate systems. Figure 18 presents the relationship between pragmatic-DDE and the L_2 norm of the density difference for this subset, evaluated across nine approximate functionals and HF. As previously noted, establishing a clear and quantitative relationship between real-space density features and DDE remains challenging. Indeed, little to no correlation is observed between pragmatic-DDE and density error metrics such as the L_1, L_2 norms, Shannon entropy[86], Fisher information[87], and Coulomb self-energy (see Figs. S9–S18). Despite extensive attempts, we failed to find any such correlation, nor have we identified any in the literature.

VI. Discussion and recent literature

To place our findings in context with previous literature, we consider specifically the barrier height of $H_2 + F \rightarrow H \cdots H \cdots F$ (and its backward reaction) as it plays a crucial role in propagating confusion about the concepts of DDEs. An earlier paper reported, based on the use of proxy benchmark densities together with the EDI, that the DDEs in HF-DFT appeared larger than those in self-consistent DFT, and therefore attributed the improved barrier heights of HF-DFT to error cancellation. In Ref.[23], one specific case was targeted for finding an accurate density and KS inversion, as a check on the value of the proxy densities. However, as both the EDI procedure and the proxy benchmark densities used in that work are not formally equivalent to the (ideal- and pragmatic-) DDE and exact densities, such conclusions are not quantitatively reliable. While our interpretation of functional contributions is not identical to that of Perdew and co-workers[20,23,25,26], both perspectives trace the key features of HF-DFT performance to the constraints and limitations inherent in the underlying approximate functional.

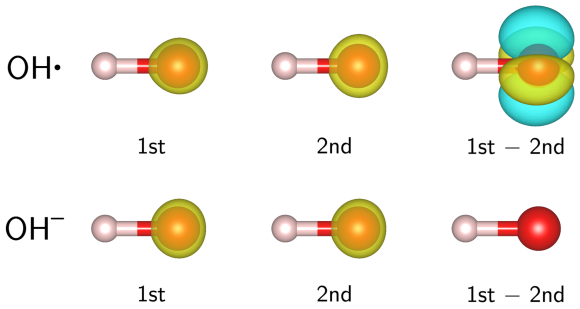

Figure 17: Electron densities and their differences between two independent PBE calculations (1st and 2nd) for the OH radical (top row) and the OH^- anion (bottom row). The OH radical exhibits substantial density variations due to degeneracy-induced random orbital occupations resulting from different self-consistent field convergence paths, whereas the closed-shell OH^- anion shows minimal differences. Yellow and cyan isosurfaces indicate positive and negative density differences, respectively. The isosurface level is set to 0.7 for individual molecular densities and 0.03 for the density differences. Quantitative comparisons of the 1st and 2nd densities for each molecule using known real-space density metrics yield the following values (in the order of OH radical, OH^- anion): $L_1 = (1.2,\ 2.0 \times 10^{-6})$, $L_2 = (0.32,\ 4.0 \times 10^{-7})$, Shannon entropy $= (2.0,\ 6.0 \times 10^{-6})$, Fisher information $= (12.6,\ 2.0 \times 10^{-5})$, and Coulomb self-energy $= (0.06,\ 3.0 \times 10^{-13})$. (See Figs. S9–S18 for the definitions of each metric.)

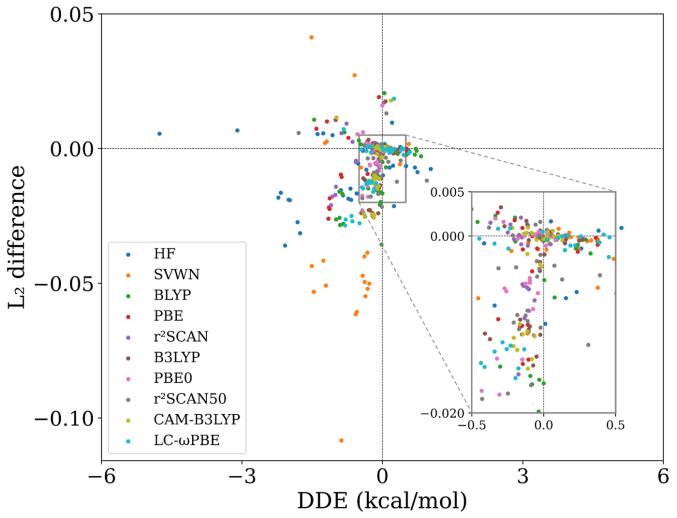

Figure 18: Relation between density-driven error (DDE) and L_2 norm differences for the 36 selected reactions (listed in Table S9), evaluated across various density functionals. CCSD densities are used as the benchmark. (See Figs. S9–S18 for additional comparisons using other density metrics, including L_1 norm, Shannon entropy, Fisher information, and Coulomb self-energy.)

Table 1 of that work reports barrier heights for that reaction, both forwards and backwards. We already showed in Sec. V1 that the proxy benchmark densities do not yet appear to achieve the precision required for quantitative pragmatic-DDE comparison (see Table 8). Nevertheless, recent proxy benchmark density approaches (Refs.[20,23,25,26]) represent important steps toward more practical benchmarks. We note that previously reported pragmatic-DDE values for HF-DFT correspond to EDIs evaluated on non-self-consistent densities, and thus are not directly comparable to the present definitions. It is unknown how large the pragmatic-DDE for those calculations is. These works nonetheless provide valuable numerical data that can inform future systematic comparisons.

But there is a crucial trend not pointed out in the paper. For every single case (7 functionals times two barrier heights), the change in barrier height from the self-consistent result to the HF-DFT result is in the same direction as the change from self-consistent to exact. Compare this with our Fig. 1 for one-electron systems, parameterized by a. Here, we do not have all densities along one line. The HF density is in some other 'direction' in density space. But the results are perfectly consistent with Fig. 1. It looks like the HF-DFT density (Eq. 14) is much closer to the exact density than the self-consistent one is, which suggests strongly that its (ideal- and pragmatic-)DDE, if we could measure it, would be smaller in magnitude than that of each of the functionals. Note that it would change from one functional to the next, but could be far less than the numbers reported in the paper. Lastly, we note that the functional error for each functional is typically larger in magnitude than the total error on the HF density, which excludes the naive interpretation of DC-DFT.[20,23,25,26,34] But this is just like Fig. 1, on the right. There's a range of densities that are more accurate than the self-consistent density, but with errors less than the functional error. Both the DDE and functional error are reduced by moving to the HF density. This is an automatic consequence of the (near) parabolic shape of the approximate functional with minimum at the self-consistent density. The naive explanation applies to the left hand side, but the right-hand side exists also. Thus, the tremendous improvement in barrier height with HF-DFT does not contradict the principles of DC-DFT. The real question is whether the DDE of such a calculation is bigger or smaller than that of the self-consistent calculation, a question we are currently unable to answer.

Table 14 gives a list of appearances of the three major sources of confusion introduced in the recent literature about DC-DFT: using EDI to decide the pragmatic-DDE of HF-DFT calculations, use of proxy benchmark densities as benchmark densities when they are not sufficiently accurate, and the idea that 'natural' metrics, such as the L_2 norm, for density errors can somehow be correlated with the measures used in DC-DFT.

Table 14: Appearance in recent literature of the energetic density interpolator (EDI), proxy benchmark densities, and scalar measures of density differences.

EDI	
Nam 2020[7]	Fig. 2, Fig. 4
Kaplan 2023[20]	Eq. 11, Table 5
Kanungo 2024[23]	Eq. 4, Table 1, Table 2
Kaplan 2024[25]	Eq. 11, Fig. 1, Fig. 3, Fig. 4, Fig. 5
Pangeni 2025[26]	Eq. 4, Table 2
proxy benchmark densities	
Kaplan 2023[20]	Eq. 10, Eq. 11, Table 5
Kanungo 2024[23]	Table 2
Kaplan 2024[25]	Eq. 6
metrics of density difference	
Medvedev 2017[54]	Fig. 1, Fig. 2, Table 1
Dasgupta 2022[11]	Eq. 9 ,Fig. 7
Shahi 2025[71]	Eq. 1

VII. Conclusions

There are many lessons to be drawn from the results presented here, lessons that are important for understanding how DC-DFT works. First, *any* work using the energetic density interpolator (EDI) yields essentially no quantitative information about density-driven errors (DDEs), and our results suggest it likely hugely overestimates DDEs. As far as we know, there are no reliable estimates of DDEs for HF-DFT (apart from those here), and there is no evidence in the literature that the HF density is less accurate than a typical self-consistent density (using the only measure that is relevant to DC-DFT). Claims of unusual or unexplained cancellations of errors between quantities labeled as "DDEs" in the literature (most of which correspond to EDI-based estimates rather than rigorous pragmatic-DDEs) and functional errors should be revisited. Our results suggest that actual DDEs of HF-DFT densities are likely much smaller than those reported, leaving no significant cancellation of errors. We emphasize that the pragmatic-DDE, as introduced in Eq. 2 of Ref.[2], was only formally defined for self-consistent densities. Therefore, to measure the pragmatic-DDE of an HF-DFT calculation, we must find the minimizing density of the functional which *self-consistently* produces the HF-DFT energy. This density, given by Eq. 14, is the true HF-DFT density. These HF-DFT densities may be quite different from the HF densities themselves, in a manner analogous to our 1-electron model in Sec. IV: where the self-consistent density of the inconsistent evaluation $\tilde{E}_{a=0}[\tilde{n}_{a=1.5}]$ is quite different from $n_{a=1.5}$. Finally, our results show that under typical circumstances, it is not surprising that often the energy error using the HF density is lower than the energy of the exact density (the functional error), and that such cases can easily occur even when the HF density is more accurate than the self-consistent density.

Two further points are worth emphasizing. First, one must be extremely careful before using proxy benchmark densities in place of benchmark densities. In general, if the proxy benchmark density does not come from a self-consistent KS calculation, we have no reliable way to estimate its pragmatic-DDE. Even if it does, and we can calculate its pragmatic-DDE, this is not a definitive yardstick for comparing one functional's density to another's, as the pragmatic-DDE depends on the functional chosen. For reasonably accurate functionals, our examples show that these are usually good proxies for ideal-DDEs, which can be compared directly (but require knowledge of the exact functional to calculate directly). Even a very small pragmatic-DDE cannot be taken as definitive evidence that the density is intrinsically accurate, and proxy benchmark densities may be too unreliable for estimating ideal-DDEs or for preserving the correct relative ordering of pragmatic-DDEs across standard functionals. Second, there are endless interesting measures of the 'accuracy' of a density, from L_2 norms to kinetic energies to Shannon entropies. We have searched hard, and found none that correlate with the pragmatic-DDE defined in DC-DFT. There are two simple reasons for this. First, DC-DFT is applied to the energy differences that are the relevant quantities in materials and quantum chemistry. There is rarely an obvious route to applying some norm over a density to differences in densities. Second, pragmatic-DDE depends on the entire functionals in an extremely complex way, so that it is unsurprising that their patterns are difficult to capture by focusing on just one single measure. Thus it seems always a mistake to conflate small density errors by one of these metrics with small ideal-DDE.

Calculation of pragmatic-DDE for a given self-consistent DFT calculation and energy difference is straightforward when a benchmark energy and density are available, provided they are sufficiently accurate. But this requires that the functional be applied self-consistently, which is not the case for HF-DFT. To find out if the HF density is more accurate by the measure of DC-DFT, requires evaluation of the exact functional on an approximate density. In general, this is impossible with present computational techniques, except for the simple cases presented here. Thus, for practical cases such as barrier heights, we cannot definitively quantify the DDE of the HF density because the EDI is unreliable for non-self-consistent calculations.

Importantly, previous works[8,20,23,25,26] provide valuable benchmark evidence regarding HF-DFT performance across a variety of systems. Our aim here is not to dispute those observations, but to clarify how such empirical findings should be interpreted within the formal DC-DFT framework.

However, what is clear is that the case of barrier heights does *not* fit the same mold as other known successes of HF-DFT. For example, for dissociation curves, it has been shown that the pragmatic-DDE dominates in the large separation limit, and

that the HF density is far better than the self-consistent density in that limit, and so almost entirely eliminates the error.[21] Neither of these statements apply to barrier heights (and perhaps other situations, too). Both existing literature[20,23,34] and our own calculations in this work clearly show that pragmatic-DDEs of self-consistent calculations do *not* dominate the errors in barrier heights, and that the improvements typically rendered by HF-DFT are significantly larger in magnitude than the pragmatic-DDE. It is plausible that the true density of an HF-DFT calculation (Eq. 14) is more accurate (i.e., has a lower ideal-DDE than the self-consistent density), as in our one-electron examples of Sec. IV1. But that would not alter the fact that the dominant improvement is in the functional-driven contribution, which is consistently and significantly smaller than its self-consistent counterpart. When exact density (here, CCSD) is evaluated on approximate functionals, the pragmatic-DDE vanishes, leaving only the functional error. Our DC-DFT analysis explains how HF-DFT can achieve lower errors than functional errors, but not why it so consistently improves barriers. Given the mild increase in multireference character of the transition state relative to reactants, it also cannot be ruled out that CCSD yields densities (not energies) that are insufficiently accurate on the scale needed for DC-DFT analysis.

We have performed a thorough DC-DFT analysis of the case of barrier heights, to the extent that is currently possible. Almost all existing evidence in the literature for the size of pragmatic-DDEs of HF-DFT and significant cancellations of errors between functional error and pragmatic-DDE is marred by the use of the unreliable DDE interpolator (or use of proxy benchmark densities). Moreover, the success of HF-DFT for barrier heights (and other cases) can still be understood within DC-DFT, by noting that an energy error in HF-DFT that is less than the functional error is not unexpected. Regardless of the relative accuracy of the HF density (which depends mightily on how you measure it), the density of an HF-DFT calculation is not the HF density. In the model case where the corresponding functional has both smaller DDE's and FE's than the original. This explains how HF-DFT can yield smaller errors than the functional error of the original functional, but sadly does not explain why it reduces most functional errors of most semilocal functionals by so much. It seems likely that further insight, combined with DC-DFT analysis, is needed.

Computational Details

The aug-cc-pV5Z[88] basis set is used for every energy and density calculations. All HF, DFT, and coupled-cluster calculations in this paper were done by PySCF[89,90] 2.9.0 version, except Figs. 8, 14, and 15, which used ORCA[91–93] 6.0.1 version and Multiwfn[94,95] to draw density contour map. Figure 17 is drawn by VESTA[96]. We set NoFrozencore option for coupled-cluster calculation in ORCA. For Kohn-Sham inversion, we use the Zhao-Morisson-Parr (ZMP)[72] algorithm in KS-pies[84] package and set 1024 for maximal λ and used Fermi-Amaldi (FA)[97] for the guiding potential.

Supporting Information

Geometries for one-electron systems, Energy curves of one-electron systems, Error distribution of DFT and HF-DFT for 103 benchmark reactions, Table of energy difference between CCSD and CCSD(T) densities, Table of subset, systems, and stoichiometry information for the 103 benchmark reactions, Table of reaction indices of the 36 selected non-degenerated reactions, Table of ideal-DDE, pragmatic-DDE, and EDI of one-electron systems, Figures of density difference contour map between CCSD and CCSD(T), Figures of relationship between DDE and real-space density metrics, Raw data of density-sensitivity, DFT, HF-DFT, coupled-cluster, and total energies for whole density-functional combinations (in XLSX).

Acknowledgments

We are grateful for the support of the National Research Foundation of Korea (NRF-RS-2025-00554671) and the Korea Environment Industry & Technology Institute (KEITI-RS-2023-00219144). S.C. acknowledges support from the UC Presidential Dissertation Year fellowship. M.S. acknowledges support from the UC Irvine Eddleman Quantum Institute Fellowship. K.B. acknowledges support from NSF grant No.CHE-2154371.

References

(1) Kohn, W.; Sham, L. J. Self-consistent equations including exchange and correlation effects. *Phys. Rev.* **1965**, *140*, A1133.

(2) Kim, M.-C.; Sim, E.; Burke, K. Understanding and reducing errors in density functional calculations. *Phys. Rev. Lett.* **2013**, *111*, 073003.

(3) Kim, M.-C.; Sim, E.; Burke, K. Communication: Avoiding unbound anions in density functional calculations. *J. Chem. Phys.* **2011**, *134*.

(4) Kim, M.-C.; Sim, E.; Burke, K. Ions in solution: Density corrected density functional theory (DC-DFT). *J. Chem. Phys.* **2014**, *140*.

(5) Kim, M.-C.; Park, H.; Son, S.; Sim, E.; Burke, K. Improved DFT potential energy surfaces via improved densities. *J. Phys. Chem. Lett.* **2015**, *6*, 3802–3807.

(6) Kim, Y.; Song, S.; Sim, E.; Burke, K. Halogen and chalcogen binding dominated by density-driven errors. *J. Phys. Chem. Lett.* **2018**, *10*, 295–301.

(7) Nam, S.; Song, S.; Sim, E.; Burke, K. Measuring density-driven errors using Kohn–Sham inversion. *J. Chem. Theory Comput.* **2020**, *16*, 5014–5023.

(8) Santra, G.; Martin, J. M. What types of chemical problems benefit from density-corrected DFT? A probe using an extensive and chemically diverse test suite. *J. Chem. Theory Comput.* **2021**, *17*, 1368–1379.

(9) Dasgupta, S.; Lambros, E.; Perdew, J. P.; Paesani, F. Elevating density functional theory to chemical accuracy for water simulations through a density-corrected many-body formalism. *Nat. Commun.* **2021**, *12*, 6359.

(10) Nam, S.; Cho, E.; Sim, E.; Burke, K. Explaining and fixing DFT failures for torsional barriers. *J. Phys. Chem. Lett.* **2021**, *12*, 2796–2804.

(11) Dasgupta, S.; Shahi, C.; Bhetwal, P.; Perdew, J. P.; Paesani, F. How good is the density-corrected SCAN functional for neutral and ionic aqueous systems, and what is so right about the Hartree–Fock density? *J. Chem. Theory Comput.* **2022**, *18*, 4745–4761.

(12) Palos, E.; Lambros, E.; Dasgupta, S.; Paesani, F. Density functional theory of water with the machine-learned DM21 functional. *J. Chem. Phys.* **2022**, *156*.

(13) Rana, B.; Coons, M. P.; Herbert, J. M. Detection and correction of delocalization errors for electron and hole polarons using density-corrected DFT. *J. Phys. Chem. Lett.* **2022**, *13*, 5275–5284.

(14) Palos, E.; Caruso, A.; Paesani, F. Consistent density functional theory-based description of ion hydration through density-corrected many-body representations. *J. Chem. Phys. 159*.

(15) Song, S.; Vuckovic, S.; Kim, Y.; Yu, H.; Sim, E.; Burke, K. Extending density functional theory with near chemical accuracy beyond pure water. *Nat. Commun.* **2023**, *14*, 799.

(16) Belleflamme, F.; Hutter, J. Radicals in aqueous solution: assessment of density-corrected SCAN functional. *Phys. Chem. Chem. Phys.* **2023**, *25*, 20817–20836.

(17) Rana, B.; Beran, G. J.; Herbert, J. M. Correcting π-delocalisation errors in conformational energies using density-corrected DFT, with application to crystal polymorphs. *Mol. Phys.* **2023**, *121*, e2138789.

(18) Morgante, P.; Autschbach, J. Density-corrected density functional theory for molecular properties. *J. Phys. Chem. Lett.* **2023**, *14*, 4983–4989.

(19) Bryenton, K. R.; Adeleke, A. A.; Dale, S. G.; Johnson, E. R. Delocalization error: The greatest outstanding challenge in density-functional theory. *Wiley Interdiscip. Rev. Comput. Mol. Sci.* **2023**, *13*, e1631.

(20) Kaplan, A. D.; Shahi, C.; Bhetwal, P.; Sah, R. K.; Perdew, J. P. Understanding density-driven errors for reaction barrier heights. *J. Chem. Theory Comput.* **2023**, *19*, 532–543.

(21) Lee, M.; Kim, B.; Sim, M.; Sogal, M.; Kim, Y.; Yu, H.; Burke, K.; Sim, E. Correcting dispersion corrections with density-corrected DFT. *J. Chem. Theory Comput.* **2024**, *20*, 7155–7167.

(22) Kim, Y.; Sim, M.; Lee, M.; Kim, S.; Song, S.; Burke, K.; Sim, E. Extending density-corrected density functional theory to large molecular systems. *J. Phys. Chem. Lett.* **2024**, *16*, 939–947.

(23) Kanungo, B.; Kaplan, A. D.; Shahi, C.; Gavini, V.; Perdew, J. P. Unconventional error cancellation explains the success of Hartree–Fock density functional theory for barrier heights. *J. Phys. Chem. Lett.* **2024**, *15*, 323–328.

(24) Broderick, D. R.; Herbert, J. M. Delocalization error poisons the density-functional many-body expansion. *Chem. Sci.* **2024**, *15*, 19893–19906.

(25) Kaplan, A. D.; Shahi, C.; Sah, R. K.; Bhetwal, P.; Kanungo, B.; Gavini, V.; Perdew, J. P. How does HF-DFT achieve chemical accuracy for water clusters? *J. Chem. Theory Comput.* **2024**, *20*, 5517–5527.

(26) Pangeni, N.; Shahi, C.; Perdew, J. P.; Subramanian, V.; Kanungo, B.; Gavini, V.; Ruzsinszky, A. Hartree-Fock density functional theory works through error cancellation for the interaction energies of halogen and chalcogen bonded complexes. *ChemRxiv* **2025**, Preprint, `https://doi.org/10.26434/chemrxiv-2025-wfft9`.

(27) Ravindran, V.; Gidopoulos, N. I.; Clark, S. J. Local exchange-correlation potentials by density inversion in solids. *Phys. Rev. B.* **2025**, *112*, 085208.

(28) Slater, J. C. A simplification of the Hartree-Fock method. *Phys. Rev.* **1951**, *81*, 385.

(29) Goerigk, L.; Hansen, A.; Bauer, C.; Ehrlich, S.; Najibi, A.; Grimme, S. A look at the density functional theory zoo with the advanced GMTKN55 database for general main group thermochemistry, kinetics and noncovalent interactions. *Phys. Chem. Chem. Phys.* **2017**, *19*, 32184–32215.

(30) Song, S.; Vuckovic, S.; Sim, E.; Burke, K. Density sensitivity of empirical functionals. *J. Phys. Chem. Lett.* **2021**, *12*, 800–807.

(31) Yu, H.; Song, S.; Nam, S.; Burke, K.; Sim, E. Density-corrected density functional theory for open shells: How to deal with spin contamination. *J. Phys. Chem. Lett.* **2023**, *14*, 9230–9237.

(32) Perdew, J. P.; Parr, R. G.; Levy, M.; Balduz Jr, J. L. Density-functional theory for fractional particle number: Derivative discontinuities of the energy. *Phys. Rev. Lett.* **1982**, *49*, 1691.

(33) Zhang, Y.; Yang, W. A challenge for density functionals: Self-interaction error increases for systems with a non-integer number of electrons. *J. Chem. Phys.* **1998**, *109*, 2604–2608.

(34) Wibowo-Teale, A. M.; Huynh, B. C.; Helgaker, T.; Tozer, D. J. Classical reaction barriers in DFT: an adiabatic-connection perspective. *J. Chem. Theory Comput.* **2024**, *21*, 124–137.

(35) Savin, A. In *Theoretical and Quantum Chemistry at the Dawn of the 21st Century*; Chakraborty, T., Carbo-Dorca, R., Eds.; Apple Academic Press, 2018; pp 645–656.

(36) Vuckovic, S.; Song, S.; Kozlowski, J.; Sim, E.; Burke, K. Density functional analysis: The theory of density-corrected DFT. *J. Chem. Theory Comput.* **2019**, *15*, 6636–6646.

(37) MacDonald, J. Successive approximations by the Rayleigh-Ritz variation method. *Phys. Rev.* **1933**, *43*, 830.

(38) Penz, M.; Tellgren, E. I.; Csirik, M. A.; Ruggenthaler, M.; Laestadius, A. The structure of density-potential mapping. Part I: Standard density-functional theory. *ACS Physical Chemistry Au* **2023**, *3*, 334–347.

(39) Lieb, E. H. Density Functionals for Coulomb Systems. *Int. J. Quantum Chem.* **1983**, *24*, 243–277.

(40) Von Barth, U.; Hedin, L. A local exchange-correlation potential for the spin polarized case. I. *J. Phys. C: Solid State Phys.* **1972**, *5*, 1629.

(41) Purvis III, G. D.; Bartlett, R. J. A full coupled-cluster singles and doubles model: The inclusion of disconnected triples. *J. Chem. Phys.* **1982**, *76*, 1910–1918.

(42) Bartlett, R. J.; Musiał, M. Coupled-cluster theory in quantum chemistry. *Rev. Mod. Phys.* **2007**, *79*, 291–352.

(43) Hernandez, D. J.; Rettig, A.; Head-Gordon, M. A new view on density corrected DFT: Can one get a better answer for a good reason? *arXiv preprint arXiv:2306.15016* **2023**,

(44) Sim, E.; Song, S.; Vuckovic, S.; Burke, K. Improving results by improving densities: Density-corrected density functional theory. *J. Am. Chem. Soc.* **2022**, *144*, 6625–6639.

(45) Gill, P. M.; Johnson, B. G.; Pople, J. A.; Frisch, M. J. An investigation of the performance of a hybrid of Hartree-Fock and density functional theory. *Int. J. Quantum Chem.* **1992**, *44*, 319–331.

(46) Oliphant, N.; Bartlett, R. J. A systematic comparison of molecular properties obtained using Hartree–Fock, a hybrid Hartree–Fock density-functional-theory, and coupled-cluster methods. *J. Chem. Phys.* **1994**, *100*, 6550–6561.

(47) Janesko, B. G.; Scuseria, G. E. Hartree–Fock orbitals significantly improve the reaction barrier heights predicted by semilocal density functionals. *J. Chem. Phys.* **2008**, *128*.

(48) Verma, P.; Perera, A.; Bartlett, R. J. Increasing the applicability of DFT I: Non-variational correlation corrections from Hartree–Fock DFT for predicting transition states. *Chem. Phys. Lett.* **2012**, *524*, 10–15.

(49) Zhang, J.; Pagotto, J.; Gould, T.; Duignan, T. T. Scalable and accurate simulation of electrolyte solutions with quantum chemical accuracy. *Mach. Learn. Sci. Technol.* **2025**,

(50) Sim, E.; Song, S.; Burke, K. Quantifying density errors in DFT. *J. Phys. Chem. Lett.* **2018**, *9*, 6385–6392.

(51) Song, S.; Vuckovic, S.; Sim, E.; Burke, K. Density-corrected DFT explained: Questions and answers. *J. Chem. Theory Comput.* **2022**, *18*, 817–827.

(52) Martín-Fernández, C.; Harvey, J. N. On the use of normalized metrics for density sensitivity analysis in DFT. *J. Phys. Chem. A* **2021**, *125*, 4639–4652.

(53) Graf, D.; Thom, A. J. Simple and efficient route toward improved energetics within the framework of density-corrected density functional theory. *J. Chem. Theory Comput.* **2023**, *19*, 5427–5438.

(54) Medvedev, M. G.; Bushmarinov, I. S.; Sun, J.; Perdew, J. P.; Lyssenko, K. A. Density functional theory is straying from the path toward the exact functional. *Science* **2017**, *355*, 49–52.

(55) Wagner, L. O.; Stoudenmire, E. M.; Burke, K.; White, S. R. Guaranteed convergence of the Kohn-Sham equations. *Phys. Rev. Lett.* **2013**, *111*, 093003.

(56) Lonsdale, D. R.; Goerigk, L. The one-electron self-interaction error in 74 density functional approximations: a case study on hydrogenic mono-and dinuclear systems. *Phys. Chem. Chem. Phys.* **2020**, *22*, 15805–15830.

(57) Lonsdale, D. R.; Goerigk, L. One-electron self-interaction error and its relationship to geometry and higher orbital occupation. *J. Chem. Phys.* **2023**, *158*.

(58) Furness, J. W.; Kaplan, A. D.; Ning, J.; Perdew, J. P.; Sun, J. Accurate and numerically efficient r2SCAN meta-generalized gradient approximation. *J. Phys. Chem. Lett.* **2020**, *11*, 8208–8215.

(59) Stephens, P. J.; Devlin, F. J.; Chabalowski, C. F.; Frisch, M. J. Ab initio calculation of vibrational absorption and circular dichroism spectra using density functional force fields. *J. Phys. Chem.* **1994**, *98*, 11623–11627.

(60) Perdew, J. P.; Burke, K.; Ernzerhof, M. Generalized gradient approximation made simple. *Phys. Rev. Lett.* **1996**, *77*, 3865.

(61) Becke, A. D. Density-functional exchange-energy approximation with correct asymptotic behavior. *Phys. Rev. A.* **1988**, *38*, 3098.

(62) Lee, C.; Yang, W.; Parr, R. G. Development of the Colle-Salvetti correlation-energy formula into a functional of the electron density. *Phys. Rev. B.* **1988**, *37*, 785.

(63) Dirac, P. A. M. Note on exchange phenomena in the Thomas atom. *Math. Proc. Camb. Philos. Soc.* **1930**, *26*, 376–385.

(64) Vosko, S. H.; Wilk, L.; Nusair, M. Accurate spin-dependent electron liquid correlation energies for local spin density calculations: a critical analysis. *Can. J. Phys.* **1980**, *58*, 1200–1211.

(65) Bursch, M.; Neugebauer, H.; Ehlert, S.; Grimme, S. Dispersion corrected r2SCAN based global hybrid functionals: r2SCANh, r2SCAN0, and r2SCAN50. *J. Chem. Phys.* **2022**, *156*.

(66) Vydrov, O. A.; Scuseria, G. E. Assessment of a long-range corrected hybrid functional. *J. Chem. Phys.* **2006**, *125*.

(67) Yanai, T.; Tew, D. P.; Handy, N. C. A new hybrid exchange–correlation functional using the Coulomb-attenuating method (CAM-B3LYP). *Chem. Phys. Lett.* **2004**, *393*, 51–57.

(68) Perdew, J. P.; Ernzerhof, M.; Burke, K. Rationale for mixing exact exchange with density functional approximations. *J. Chem. Phys.* **1996**, *105*, 9982–9985.

(69) Szabo, A.; Ostlund, N. *Modern Quantum Chemistry: Introduction to Advanced Electronic Structure Theory*; Dover Books on Chemistry; Dover Publications, 1996.

(70) Görling, A.; Levy, M. Correlation-energy functional and its high-density limit obtained from a coupling-constant perturbation expansion. *Phys. Rev. B.* **1993**, *47*, 13105.

(71) Shahi, C.; Perdew, J. P. Comment on "Comment on "Accurate correlation potentials from the self-consistent random phase approximation". *Phys. Rev. Lett.* **2025**, *135*, 019601.

(72) Zhao, Q.; Morrison, R. C.; Parr, R. G. From electron densities to Kohn-Sham kinetic energies, orbital energies, exchange-correlation potentials, and exchange-correlation energies. *Phys. Rev. A.* **1994**, *50*, 2138.

(73) Wu, Q.; Yang, W. A direct optimization method for calculating density functionals and exchange–correlation potentials from electron densities. *J. Chem. Phys.* **2003**, *118*, 2498–2509.

(74) Shi, Y.; Wasserman, A. Inverse Kohn–Sham density functional theory: Progress and challenges. *J. Phys. Chem. Lett.* **2021**, *12*, 5308–5318.

(75) Gould, T. Toward routine Kohn–Sham inversion using the "Lieb-response" approach. *J. Chem. Phys.* **2023**, *158*.

(76) Callow, T. J.; Lathiotakis, N. N.; Gidopoulos, N. I. Density-inversion method for the Kohn–Sham potential: Role of the screening density. *J. Chem. Phys.* **2020**, *152*.

(77) Erhard, J.; Trushin, E.; Görling, A. Numerically stable inversion approach to construct Kohn–Sham potentials for given electron densities within a Gaussian basis set framework. *J. Chem. Phys.* **2022**, *156*.

(78) Erhard, J.; Trushin, E.; Görling, A. Kohn–Sham inversion for open-shell systems. *J. Chem. Phys.* **2025**, *162*.

(79) Takahashi, H. Comparison of optimized effective potential with inverse Kohn–Sham method for Hartree–Fock exchange energy. *J. Chem. Phys.* **2024**, *161*.

(80) Kanungo, B.; Zimmerman, P. M.; Gavini, V. Exact exchange-correlation potentials from ground-state electron densities. *Nat. Commun.* **2019**, *10*, 4497.

(81) Sun, J.; Ruzsinszky, A.; Perdew, J. P. Strongly constrained and appropriately normed semilocal density functional. *Phys. Rev. Lett.* **2015**, *115*, 036402.

(82) Watts, J. D.; Gauss, J.; Bartlett, R. J. Coupled-cluster methods with noniterative triple excitations for restricted open-shell Hartree–Fock and other general single determinant reference functions. Energies and analytical gradients. *J. Chem. Phys.* **1993**, *98*, 8718–8733.

(83) Scuseria, G. E. Analytic evaluation of energy gradients for the singles and doubles coupled cluster method including perturbative triple excitations: Theory and applications to FOOF and Cr2. *J. Chem. Phys.* **1991**, *94*, 442–447.

(84) Nam, S.; McCarty, R. J.; Park, H.; Sim, E. KS-pies: Kohn–Sham inversion toolkit. *J. Chem. Phys.* **2021**, *154*.

(85) Bauza, A.; Alkorta, I.; Frontera, A.; Elguero, J. On the reliability of pure and hybrid DFT methods for the evaluation of halogen, chalcogen, and pnicogen bonds involving anionic and neutral electron donors. *J. Chem. Theory Comput.* **2013**, *9*, 5201–5210.

(86) Shannon, C. E. A mathematical theory of communication. *Bell Syst. Tech. J.* **1948**, *27*, 379–423.

(87) Fisher, R. A. Theory of Statistical Estimation. *Math. Proc. Camb. Philos. Soc.* **1925**, *22*, 700–725.

(88) Dunning Jr, T. H. Gaussian basis sets for use in correlated molecular calculations. I. The atoms boron through neon and hydrogen. *J. Chem. Phys.* **1989**, *90*, 1007–1023.

(89) Sun, Q.; Berkelbach, T. C.; Blunt, N. S.; Booth, G. H.; Guo, S.; Li, Z.; Liu, J.; McClain, J. D.; Sayfutyarova, E. R.; Sharma, S.; others PySCF: the Python-based simulations of chemistry framework. *Wiley Interdiscip. Rev. Comput. Mol. Sci.* **2018**, *8*, e1340.

(90) Sun, Q.; Zhang, X.; Banerjee, S.; Bao, P.; Barbry, M.; Blunt, N. S.; Bogdanov, N. A.; Booth, G. H.; Chen, J.; Cui, Z.-H.; others Recent developments in the PySCF program package. *J. Chem. Phys.* **2020**, *153*.

(91) Neese, F. The ORCA program system. *Wiley Interdiscip. Rev. Comput. Mol. Sci.* **2012**, *2*, 73–78.

(92) Neese, F. Software update: the ORCA program system, version 4.0. *Wiley Interdiscip. Rev. Comput. Mol. Sci.* **2018**, *8*, e1327.

(93) Neese, F.; Wennmohs, F.; Becker, U.; Riplinger, C. The ORCA quantum chemistry program package. *J. Chem. Phys.* **2020**, *152*.

(94) Lu, T.; Chen, F. Multiwfn: A multifunctional wavefunction analyzer. *J. Comput. Chem.* **2012**, *33*, 580–592.

(95) Lu, T. A comprehensive electron wavefunction analysis toolbox for chemists, Multiwfn. *J. Chem. Phys.* **2024**, *161*.

(96) Momma, K.; Izumi, F. VESTA: a three-dimensional visualization system for electronic and structural analysis. *J. Appl. Cryst.* **2008**, *41*, 653–658.

(97) Fermi, E.; Amaldi, E. *Le orbite [infinito] s degli elementi*; Reale Accademia d'Italia, 1934.